Yıldırım, Halid Can; Remes, Heikki; Nussbaumer, Alain

Fatigue properties of as-welded and post-weld-treated high-strength steel joints

Published in:
International Journal of Fatigue

DOI:
10.1016/j.ijfatigue.2020.105687

Published: 01/09/2020

Document Version
Peer-reviewed accepted author manuscript, also known as Final accepted manuscript or Post-print

Fatigue properties of as-welded and post-weld-treated high-strength steel joints: The influence of constant and variable amplitude loads

Halid Can Yıldırım[a,1], Heikki Remes[b], Alain Nussbaumer[c]

[a] *Aarhus University, Department of Engineering, Aarhus, Denmark*

[b] *Aalto University, Department of Mechanical Engineering, Espoo, Finland*

[c] *Swiss Federal Institute of Technology in Lausanne, Civil Engineering, RESSLab, Switzerland*

Abstract

In HSS welded structures, HFMI allows fatigue strength improvement factors by inducing compressive residual stresses, cold-worked surface region and modifying the weld toe shape. According to the literature, the factors are proposed based on failures at CAL and also checked with a limited dataset at VAL, the latter being more realistic of service loadings. Therefore, this paper investigates the behaviour of HFMI welds at CAL and VAL for R= -0.43. Studies are also performed at the microstructural level for locating the crack initiation and hardness. Fatigue damage sums are evaluated and discussed with the recommended values in the literature.

Keywords:
Fatigue strength improvement, high-frequency mechanical impact treatment, high-strength steel, service loading

Nomenclature

[1] halid.yildirim@eng.au.dk

f_y	Yield strength
k	Number of specimens in series
AW	as-welded
CAL	Constant amplitude loading
VAL	Variable amplitude loading
FAT	The IIW fatigue class, i.e. the nominal stress range in mega pascals corresponding to 95% survival probability at 2×10^6 cycles to failure (a discrete variable with 10-15% increase in stress between steps
IIW	International Institute of Welding
HSS	High strength steels
HFMI	High frequency mechanical impact
HAZ	Heat affected zone
$\Delta\sigma$	Stress range
k	slope of the Woehler- or Gassner-line
k^*	slope of the Woehler-line after the knee point for constant amplitude loading
$k^{'}$	slope of the Woehler-line after the knee point for cumulative damage calculation
P_s	Probability of survival
R	load or stress ratio ($R = F_{min}/F_{max}$ or $\sigma_{min}/\sigma_{max}$)
N	Number of cycles
SD	Standard deviation
e	Axial misalignment
α	Angular misalignment
k_m	stress magnification coefficient

subscripts

a	amplitude
al	allowable
an	nominal amplitude
k	knee point of the Woehler-line
f	failure
n	nominal
th	theoretical

1. Introduction

During their service life, components and structures are subject to severe cyclic and dynamic loading, which may result in fatigue damage at welded joints where local stress concentrations are relatively high due to the joint geometry, e.g. weld toes and roots, and tensile residual stresses [1]. In order to overcome this effect, researchers have suggested several thermal and mechanical post-weld treatment techniques to overcome fatigue damage at welded joints [2]. These techniques rely on improving the stress field and/or the surface geometry in and around the welds. Some of these techniques are applied during the welding process, e.g., by weld profile control or using special electrodes, whereas some of them are performed as separate work operations after the welding process, e.g. post-weld treatment. Particularly, post-weld treatment methods are generally known to be beneficial and they have been considered in design regulations and guidelines [3] [4] [5].

High-frequency mechanical impact (HFMI) is a novel, reliable and effective way of improving the fatigue strength improvement for welded structures as a post-weld treatment method[5][6][7]. Ultrasonic impact treatment (UIT), ultrasonic peening (UP), ultrasonic peening treatment (UPT), high frequency impact treatment (HiFiT), pneumatic impact treatment (PIT), and ultrasonic needle peening (UNP) are a few of the HFMI devices described in the literature. In HFMI, cylindrical indenters are accelerated against a component or structure at the potential fatigue crack initiation sites with high frequency (>90Hz). The cylindrical indenters can be in different diameters and be single or multiple depending on the manufacturer of the device and purpose of use. Typical range of pin radii of HFMI indenters is 2-8mm. Different power sources such as, ultrasonic piezoelectric elements, ultrasonic magnetostrictive elements, or compressed air are used. The benefits of HFMI treatment for welded joints are considered to be derived from the imposed beneficial compressive residual stress state near the weld toe, and the establishment of a smooth transition from parent material to the weld metal as well as cold-worked surface region. According to recent studies, fatigue performance of HFMI-treated welded details increases as the yield strength (f_y) of base material increases [8].

So far in the literature, HFMI studies have mainly focused on the degree of improvement in fatigue strength at constant amplitude loading (CAL) [9] [5] [10]. Studies dealing with HFMI material characterization have also been performed in a limited manner including the investigations on highly cold-worked region [11], hardness dependency on steel strength [12], influence of operating parameters [13] and the microstructure after fatigue loading [14]. A study by Khurshid et al. discussed the stability of HFMI-induced stresses [15], they have measured surface residual stresses of four specimens and observed that compressive residual stresses are quite stable with some relaxation at fatigue loading, only limited to the CAL. Mikkola and Marquis have also shown that HFMI treatment increases the fatigue life of un-welded steel under low applied strains [16]. On the contrary the treatment may decrease the fatigue life at high-applied strains. Based on the numerical simulations, Mikkola et al. [17] [9] have shown that full residual stress relaxation may occur at CAL for $R = 0.5$ and a compressive peak stress of $0.6f_y$. Nevertheless, improvement in fatigue strength could be expected even after significant residual stress relaxation due to work hardening and modification of weld to profile. For instance, Schubnell et al. [18] have shown that the effect of work hardening may result in significant fatigue life improvement for S355 mild steel. Additionally, the study of Mikkola et al. [9], considering S700 steel, has indicated that benefit from HFMI could be still expected due to improved weld geometry and strain hardening even full stress relaxation has been observed at $R = 0.5$.

In real situations, structures may be subject to severe cyclic and dynamic loading at service, which are classified as a variable amplitude loading (VAL) rather than being a CAL. During VAL, there are a number of special phenomena that are not observed for CAL. Tensile overloads may

interact with other mechanisms such as yielding or fracture while compressive overloads may have significant influence on local buckling, relaxing the induced stress field or producing secondary bending stresses and eventually affect the fatigue properties of welds, such as damage and failure mode. With that in mind, the aim of this paper is to investigate the benefits of HFMI treatment for high strength steel welds at VAL. Investigations have been carried out for two different types of steel grades with $f_y = 423$ MPa and $f_y = 832$ MPa, as the pronounced treatment and its benefits are believed to be depended on the material strength.

2. Methods

2.1. Experiments

2.1.1. Material and Test samples

Materials considered in this work are AH36 and S690QL steel grades having 6 mm of thickness, which were provided by SSAB in Finland. Reported mechanical properties and chemical composition for each steel grade are presented in Tables 1 and 2. To produce the specimens, the manufacturing of the welded plates was performed using robot welding at Meyer Turku Shipyard in Finland. Test specimens used in this study were transverse non-load carrying attachments with fillet welds as shown in Figure 1 and Figure 17. Welding was performed with TURBOD 14.12 for AH36 and TURBOD 15.09 for S690QL with heat input parameters in the range of 0.66-0.77 kJ/mm.

Table 1: Mechanical properties of materials AH36 and S690QL.

Material	f_y [MPa] min	f_U [MPa]	Elongation (%), minimum	Impact strength J at -40°C, average minimum
AH36 [19]	423	546	0	0
S690QL [20]	832	856	0	75

Table 2: Chemical composition of materials (in percent) ladle analysis, maximum values

Material	C	Si	Mn	P	S	Al	Nb	V	Ti	Cu	Cr	Ni	Mo	Ca	B	EW
AH36 [19]	0.14	0.39	1.43	0.008	0.007	0.034	0.013	0.008	0.04	0.021	0.08	0.06	0.007	0.0	NA	NA
S690QL [20]	0.14	0.29	1.21	0.011	0.001	0.047	0.021	0.028	0.10	0.01	0.28	0.05	0.150	0.0	0.002	0.43

2.1.2. Post-weld treatment

Post-weld treatment was performed by HFMI manufacturer SONATS in France on the four welded plates. Indenters with a round tip radius of 1.5 mm were used at the weld toe region for both steel grades. Size of the treated plates was 8000 mm in length and 600 mm in width. During the HFMI treatment, the experts chose to place the peening head (1) at the junction of the base material and the weld, (2) at the half of the angle formed by the base pate and the weld seam and (3) perpendicular to the weld toe. These indications are shown in Figures 2 and 3. Welded plates were then cut at the Materials Laboratory of Aalto University in pieces to obtain small-scale specimens. Prior to fatigue testing, specimens were polished at the edges.

2.2. Geometry measurements

Geometry measurements were carried out with an ATOS Scanbox from GmbH having an optical measuring system with an accuracy of 0.02 mm [21]. The measuring system included two high resolution cameras, which recorded the geometry points on the top of the specimen surface to obtain the 3D models. The small-scale specimens were measured from both sides to capture the plate distortion and the weld shape. From each 3D model, ten of 2D sections at every 4 mm from the edge of the sample perpendicular to the weld seam were generated and analysed, see Section 3.1.

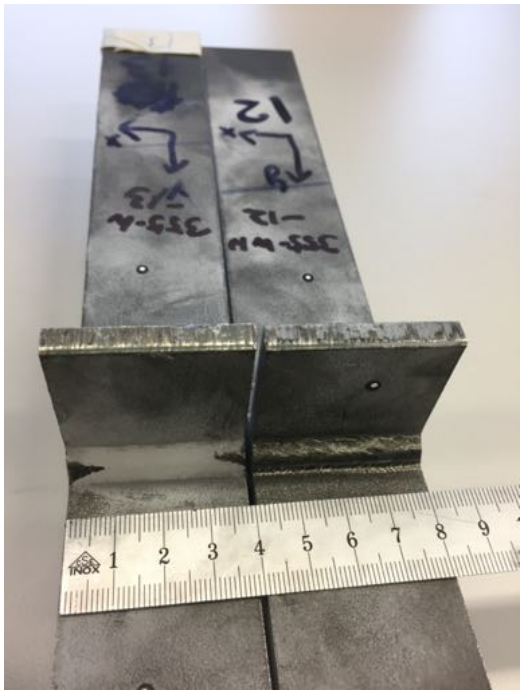

(a) Test specimens in the as-welded (left) and HFMI-treated (right) conditions

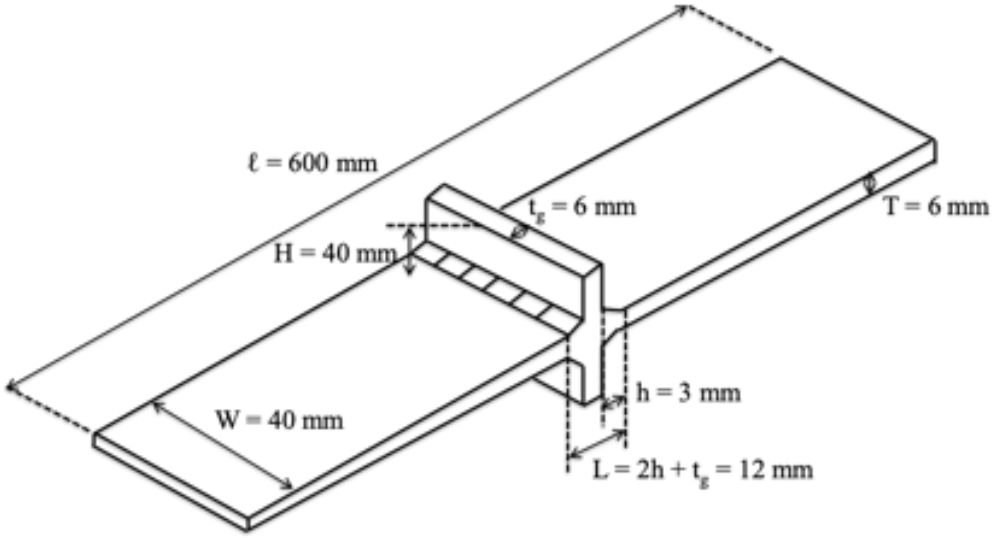

(b) Schematic view of the test specimen

Figure 1: Transverse non-load carrying attachments

2.3. Microstructural investigations and hardness measurements

Samples for microhardness measurements and microstructure analysis were extracted from each steel grade and each conditions. Macrographs were taken using an optical microscope, whereas microhardness was measured using an instrumented Vickers hardness test device and load of 1000 gf equivalent to HV1. The samples were prepared by cutting with a water-cooled abrasive disc cutter, and then grinded through P180 to P2400 grit. Polishing was carried out with $3\mu m$ and $1\mu m$ diamond prior to hardness measurements. Samples were etched with 2% Nital solution after hardness measurement to reveal the microstructure. Level of etching varies slightly

(a) Creation of a controlled radius at the weld toe

(b) Introduction of residual compressive stresses by HFMI

Figure 2: Application and resulted effect of the used HFMI technology

between specimens, and thus the appearance of same microstructural constituents can be different.

Hardness was measured on one side of the transverse cross-section, following the edge of the sample from the attached side plate, over the HAZ and the weld metal and up to the base plate. In addition, hardness was measured at the weld root. The measurements were taken at a distance of 0.3 mm from the edge of the plate or weld metal in order to avoid edge effects and work-hardened regions. The distance between measurement points was 0.3 mm or 0.6 mm.

2.4. Fatigue testing and spectrum loading

The specimens were fatigue tested under load-controlled axial loading in hydraulic fatigue testing machines. In total, 35 specimens for AH36 and for S690QL were fatigue tested at CAL or VAL at the Resilient Steel Structures Laboratory (RESSLab) at EPFL. The used machine was an Instron Schenck universal machine with a fatigue load capacity of 800 kN. Additionally, 38 specimens were also fatigue tested under CAL at the Mechanics of Materials Laboratory at Aalto University by using an MTS test machine with fatigue load capacity of 250 kN. For both steel grades, an identical variable amplitude loading history is used with a stress ratio of $R = -0.43$. Anti-buckling supports, which were manufactured from the high strength steel plates, were fitted around the specimens in order to avoid the risk of buckling during the relatively large compressive loads occurring regularly in the spectrum. Teflon sheets were also used in between the buckling supports and sample in order to minimize friction.

Variable amplitude loading considered in this study has shown its effectiveness in a previous study by Yıldırım and Marquis [22]. For the VAL, a cycle extract and cumulative cycle distribution are shown in Fig 4. The loading history included 250,000 cycles distributed between fourteen different amplitudes. The cycle amplitude distribution was approximately linearly distributed on a semi-log plot. The amplitude of the smallest applied load cycle was 16 % of the maximum load cycle. The order of the individual cycles within the 250,000 spectrum was randomly chosen and each cycle had a stress ratio of $R = -0.43$. Here, the aim was to perform fatigue testing at a stress ratio that would provide considerable amount of residual stresses relaxation and would avoid buckling of specimens under overloads close to the yield strength of material. For the constant amplitude loading, fatigue testing was carried out at two different stress ratios: firstly at $R = 0.1$ to ensure that the weld quality is within the range of standards, secondly at $R = -0.43$ to make the comparison with the results at VAL. Depending on the load range, fatigue tests were performed at an average cyclic frequency of around 4-10 Hz at EPFL and 20 HZ at Aalto, for VAL and CAL respectively. During the testing, the applied load history was continuously monitored to ensure that the desired history matched the true applied history.

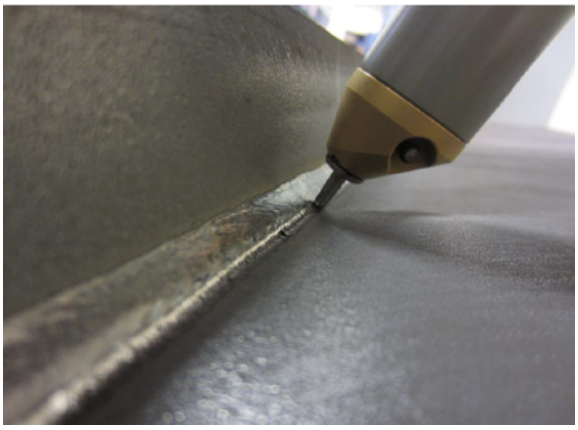

(a) Intender location during the treatment

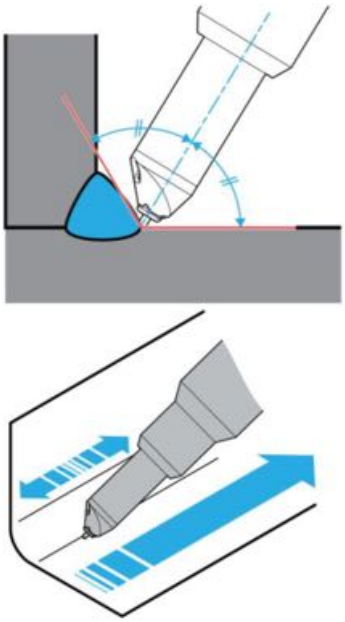

(b) Position (up) and movement of the peening (down) during the HFMI treatment

Figure 3: Position of the HFMI tool during the treatment

2.5. Residual stress measurements

For both as-welded and HFMI-treated conditions, investigations to map the residual stress state of the joints were performed by neutron scattering through the thickness at The Forschungs-Neutronenquelle Heinz Maier-Leibnitz (FRM II), Technical University of Munich, Germany and at The Institut Laue–Langevin (ILL) in Grenoble, France. Surface residual stress were measured by the instrument called STRESS SPEC in Germany [23], whereas in depth measurements were done by SALSA in France [24]. Both instruments were specifically developed and designed for the study of residual stresses.

Residual stress or strain measurements by neutron diffraction method requires investigations on at least two types of samples. The first is the reference sample, the second is the sample under investigation, where the former one provides the necessary information that characterises the material in its residual stress free state. For this, small 1.75 mm cubes, representative of the material at the different analysed depths, were cut from the selected specimens by electric discharge machining at the Workshop ATMX at EPFL. In this study, the procedure presented in

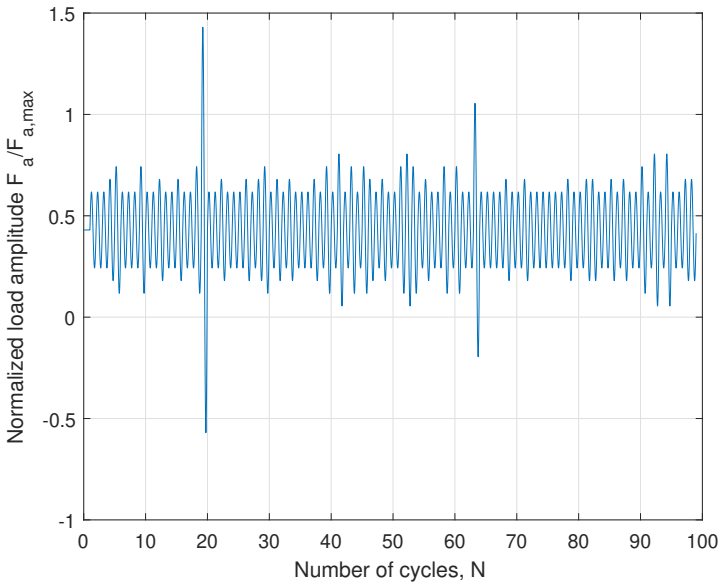

(a) Sample from one short segment of the spectrum, around 100 cycles

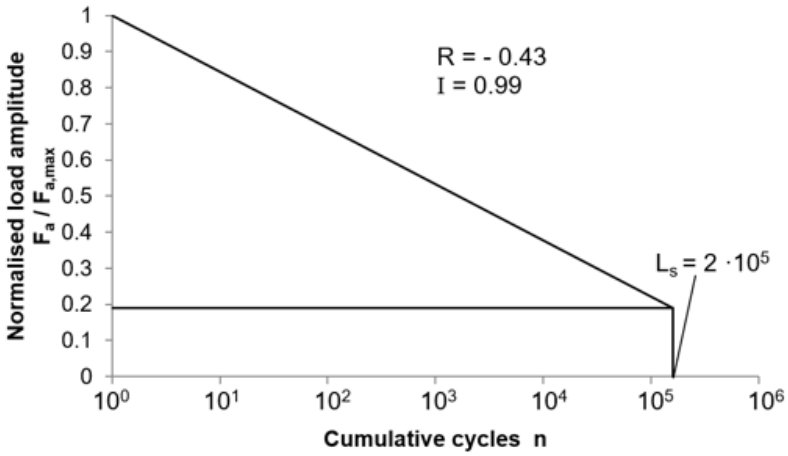

(b) Load sequence of the cumulative amplitude distribution

Figure 4: Details of applied variable amplitude loading spectrum

Nobre et. al [25]was followed to get the reference samples. Reference samples were manufactured from both the as-welded and HFMI-treated conditions. Only one transverse non-load carrying specimen manufactured from AH36 steel grade was measured due to the limited time at the neutron diffraction facility provider. Given the 72 hours of beam time, only before and after the HFMI treatment conditions of the specimens were measured.

3. Results and discussion

3.1. Geometry measurements

Geometry measurements aimed at comparing the fatigue test result with the weld and joint shapes, where cracking occurred, and the amount of misalignments was reported for each specimen in each series. Figure 5 presents the angular misalignment and sign rule used in the analysis.

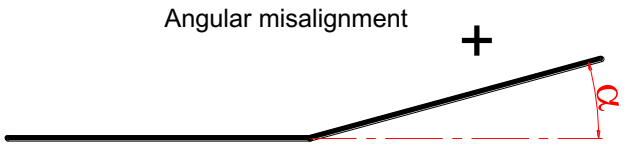

Figure 5: Sign rule for the angular misalignment.

3.1.1. *Measurement of angular misalignment*

Figure 6 presents the average, the maximum and the minimum values of angular misalignments for each series. The measurements included 4 different test series. In total 89 test specimens were measured. For S690QL grade, 25 and 24 of as-welded and HFMI-treated, respectively. For AH36 grade, forty specimens in as-welded and HFMI-treated conditions were measured. For each specimen, at least 10 measurements were taken at the sections to define the misalignment values.

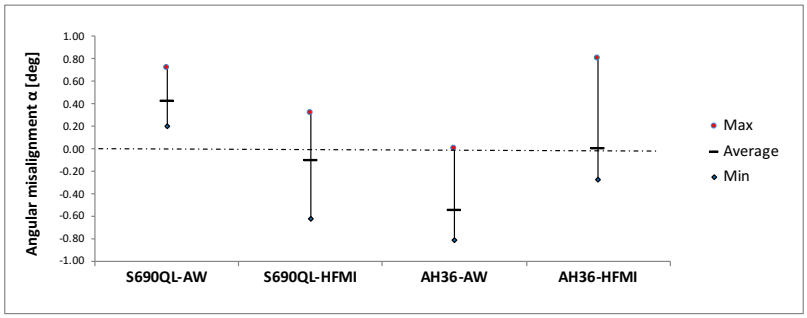

Figure 6: Angular misalignment values of transverse non-load carrying attachments as a function of specimen type.

The absolute values of angular misalignment are between 0 and 0.81 degree. The largest uncertainty in angular misalignment was found in the as-welded state of AH36 joint. However, the HFMI treated joints have significant different misalignment values in comparison to as-welded joints. This difference in angular misalignments can result from the HFMI treatment process, since the change between as-welded and HFMI treatment is clearly recognizable for both AH36 and S690QL steel grades. The change between individual as-welded specimen of the same type can be caused during the welding process itself or sample cutting.

3.1.2. *Stress magnification coefficient*

The angular misalignment influence on fatigue life was further studied by calculating the stress magnification coefficient, see Equation 1 for k_m.

$$k_m = 1 + \frac{3\alpha l}{2t} \tag{1}$$

In Equation 1 α is the angle of misalignment, l is half the full length (one plate) and t is the main plate thickness [3].

Figure 7 shows the average k_m values of the different specimen types. When comparing Figure 6 and Figure 7, one sees that the k_m value is in direct relation with α, since k_m is a function of angular misalignment. As earlier noticed, specimens manufactured from AH36 steel grades have the largest variation also in stress magnification factors. Since the as-welded joints with AH36 grade has only negative angle, the differences between maximum and minimum is the largest.

This varies from $1 < k_m < 1.41$ with an average of 1.28. The HFMI-treated specimen has the second largest variation ($1 < k_m < 1.4$) with a lower average value of 1.09, indicating for a less severe effect of angular misalignment than for non-treated welds.

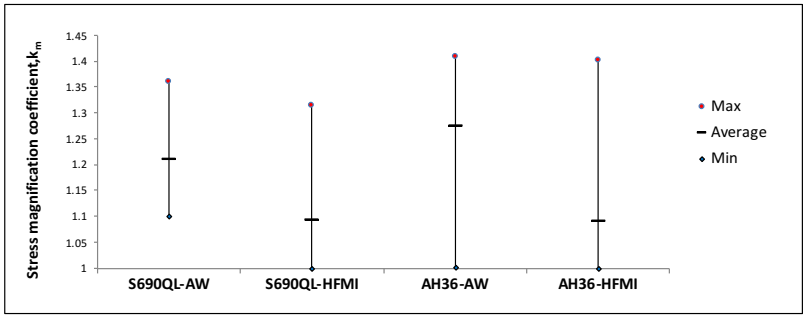

Figure 7: Stress magnification k_m values for non-load carrying transverse attachments as a function of specimen groups.

The k_m results are next compared to the value from the design guidelines. According to the Recommendations for Fatigue Design of Welded Joints and Components [3], the stress magnification coefficient in nominal stress approach is already included in the different FAT classes. The k_m value in this approach is 1.25, for the case of fillet welds on both plate sides. Comparing the results to the nominal stress coefficient, one of the average is found to be higher, namely for the as-welded specimens in AH36 steel grade. Given that $k_{m,calculated} > k_{m,nominal}$, the specimen fatigue strength results should fall below the FAT class in comparison other specimen groups, for the nominal stress approach.

3.2. Microstructural investigations and hardness measurements

The microstructural investigations were carried out for AH36 and S690QL steel joints in the as-welded and HFMI-treated conditions. All samples were untested, except for AH36 HFMI, which was an interrupted test specimen at $N = 1 \times 10^7$.

3.2.1. AH36 joints in as-welded and HFMI-treated conditions

The macrosection and micrograph of as-welded and HFMI-treated AH36 joints are shown in Figures 8a and 8b, respectively. The sequence of welding is apparent with two distinctly different microstructures observed for the weld beads. The ones having a lighter shade (5,6,7,8) were welded first, and the microstructure was annealed by the second weld beads (1,2,3,4). The microstructures of the left side weld bead are also shown at 100x magnification in these figure below. For the AH36 joint in as-welded condition, the weld metal has a very fined grained structure with a quite uniform grain size. Adjacent to the fusion line there is a layer containing a large volume fraction of martensite. This layer has been annealed in the other weld beads. This section of the HAZ is followed by the fine-grained and intercritical head-affected zones.

For the AH36 joint with HFMI treatment, the specimen is seen mounted in epoxy in a different orientation, as the last weld passes are now on the top-right and bottom-left quadrants. There are notable differences to the as-welded condition. The shape of the weld beads is irregular, with two of the welds (top-left, bottom-right) showing concavity on the surface. Furthermore, there are sharp lips/corners, possibly produced by the HFMI-treatment. In addition, the penetration depth of the welds, particularly the final beads (top-right, bottom-left) is extremely shallow in the load carrying plate in comparison to the as-welded specimen. This may have contributed to the differences observed in the hardness profiles as well. The micrograph in Figure 8b below shows a microstructure similar to the as-welded joint, except for the annealing effect on the HAZ.

Hardness measurement results for AH36 steel are shown in Figure 8. The corresponding numbers indicate the measurement locations and directions. For the as-welded condition in Figure 8a, the largest measured hardness values (339,335 HV1) are located in the martensitic HAZ on the left side weld bead. The annealed weld on the right side has notably lower hardness values, with a peak hardness of 265 HV1. The mean hardness of the base plates is 186 HV1 and of the weld metal 242 HV1. In general the hardness profile is good, and the peak hardness in the HAZ is well in the acceptable range as given by the DNV-GL guideline (<380 HV [26]).

For the HFMI-treated conditions 8b, the hardness values are higher than for the as-welded joint. The first observation is that the hardness of the load-carrying plate (201 HV1) is significantly higher than the non load-carrying plates (186 HV1). For the as-welded specimen both plates have the hardness of 186 HV1. Thus it is possible that the L-C plate has a different chemical composition, with possibly higher carbon-equivalent-value (CEV) leading to hardening of the material. Peak hardness values in HAZ are also significantly higher, with the annealed weld (top-left) having a peak hardness of 308 HV1, and the last weld bead a peak of 422 HV1. This is considerably higher than the peak of 338 HV1 observed for the as-welded specimen, and significantly above the 380 HV guideline [26]. Weld metal hardness is also up to 263 HV1 from 241 HV1. As the sample was manufactured from a runout specimen, it is possible that there is cyclic hardening contributing to this increase of weld hardness. Weld bead placement may also have influences the difference in hardness profile. It is recommended that the welding parameters and materials used for the HFMI–treated specimens are checked.

3.2.2. S690QL joints in as-welded and HFMI-treated conditions

The macrograph and micrograph of the S690QL specimens are shown in Figure 9. For the as-welded condition in Figure 9a, the size of the welds as well as their penetration depth is much smaller compared to the AH36 specimens. As a result the heat-affected zones are smaller, and seem to have a slightly smaller effect on the prior weld beads. This is reflected in the hardness characteristics. In general the weld toes have a smooth transition from the base metal even in the as-welded state. A typical microstructure is shown in Figure 9a below. It is difficult to determine the exact composition of the base metal, but it appears to be a mixture of bainite and martensite. The three heat-affected zones are apparent from left to right: Intercritical, fine-grained and coarse grained. Weld metal is fine grained, with some bainite or martensite (brownish tint in the micrograph).

In the case of HFMI treated condition in Figure 9b, the sample was etched more than the as-welded specimen, which changed especially the appearance of the welds at this low magnification. The solidification structure of the welds becomes more apparent. The weld is very similar to the as-welded specimen, with the notable difference being the worse fit-up of the non-load carrying plates. The microstructure shown in Figure 9b below is also very similar to the as-welded case.

The hardness profiles are shown in Figure 9. For the as-welded case in Figure 9a, the left and right side welds show very similar trends, with peak hardness values of 390 HV1 in the heat affected zone. Some annealing has taken place on the right side weld HAZ (Location 8, coordinate 0 – 2 mm) with peak hardness of 361 HV1 compared to 390 HV1 on the left side (Location 4, 3.5 – 5 mm). The base metal mean hardness is 282 HV1, with weld metal evenly matched at 306 HV1.

In the case of HFMI-treated condition in Figure 9b, the profiles and mean values are nearly identical to the as-welded specimen. The peak HAZ hardness values are slightly higher at 403 HV1 and 396 HV1 compared to the 390 HV1 of the as-welded specimen. However, the difference is very small, and can be caused by slight differences in indentation location. Furthermore, differences of this magnitude are within experimental error.

3.3. Fatigue testing

Fatigue test results obtained at $R = -0.43$ are presented in Figures 10 and 11 and reported in Appendix B in Tables 13 and 14 for AH36 and S690QL steels, respectively. In both figures, solid and empty data points show the fatigue testing performed for HFMI-treated and as-welded conditions of joints, respectively. Run-out or interrupted test results were not included in the analyses however they are indicated with an arrow next to the data point.

It is worth to note that the basis for the evaluation of the test results are the Woehler-lines obtained at CAL (rectangular spectrum) and the Gassner-lines determined at VAL (straight-line spectrum) for the two investigated material states, namely for as-welded and HFMI-treated conditions. The results in Figures 10 and 11 consider the maximum applied stress to show the greatest benefits of considering VAL in fatigue testing as compared to CAL. Two series of fatigue testing at CAL were also performed at $R = 0.1$ in order to demonstrate and verify the weld quality in the as-welded condition for AH36 and S690QL steel grades. The data points for these series are marked with grey colors in Figures 10 and 11. The obtained results validate the weld quality as their observed fatigue strengths are all well-above the IIW recommended value of 80 MPa for transverse non-load carrying welds [3].

The test results shown in Figures 10 and 11 were analysed according to the recommended slopes by Yıldırım [10] and the best-fit slopes separately, see Tables 3 4 5 and 6. In all these evaluations, three-parameter Weibull distribution was used to calculate the characteristic and median fatigue strengths, which represent the values at 95% and 50% of survival probability. On one hand, there is good agreement is seen between the recommended and best-fit slopes of analysed data of joints in the as-welded conditions, both at VAL and CAL for $R = -0.43$. In the case of welds with HFMI treatment, on the other hand, the best-fit slopes are larger than the recommended value of 5.6, except for the tests at CAL for $R = -0.43$.

In the case of HFMI-treated joints, calculated fatigue strength values are found to be well above the IIW recommended FAT values of 140 MPa and 180 MPa for grades 355 MPa $< f_y \leq$ 550 MPa and 750 MPa $< f_y \leq$ 950 MPa, respectively [4]. For the as-welded conditions, test results indicate that weld quality is well satisfied as the characteristic values are above the IIW recommended value of FAT 80.

For the variable amplitude loading, the total counted cycles correspond to the repetition of the history of the cycles after omission. The knee-point of the Woehler-lines is at $N = 1 \times 10^7$ cycles and the curve should continue on the basis of a further decline in stress range of about 10% per decade in terms of cycles, which corresponds to a slope of $k^* = 22$ [3] [27]. The slopes of the Woehler- and Gassner-lines above the knee-points were determined by linear regression at their mean values with the slopes of k=5.6 and k=4.0 for HFMI-treated and as-welded conditions, respectively, based on the previous observations [28]. The shallower slopes of the HFMI-treated joints result from the fact that, at higher stress levels, the beneficial compressive residual stresses near the weld toe experience more shakedown due to localised reversed plasticity than at lower stress levels [28][5]. This results in shorter lives (less improvement) at higher stress ranges then at lower ones, and thus to shallower slopes for HFMI treated joints are obtained as compared to the as-welded ones.

Table 3: Statistical analyses of fatigue test results for AH36 steel at CAL $R = -0.43$ in as-welded and HFMI treated conditions

	HFMI		As-welded	
	fixed slope	free slope	fixed slope	free slope
k :	5.6	3.1	4	4.5
$\Delta\sigma_n$ [50%] in MPa	171	163	142	148
$\Delta\sigma_n$ [95%] in MPa	169	145	136	146
SD	0.19	0.1	0.05	0.02

Table 4: Statistical analyses of fatigue test results for AH36 steel at VAL $R = -0.43$ in as-welded and HFMI treated conditions

	HFMI		As-welded	
	fixed slope	free slope	fixed slope	free slope
k :	5.6	6.4	4	4.1
$\Delta\sigma_n$ [50%] in MPa	607	600	507	509
$\Delta\sigma_n$ [95%] in MPa	554	573	472	470
SD	0.18	0.16	0.08	0.08

Table 5: Statistical analyses of fatigue test results for S690QL steel at CAL $R = -0.43$ in as-welded and HFMI treated conditions

	HFMI		As-welded	
	fixed slope	free slope	fixed slope	free slope
k :	5.6	9.4	4	4.5
$\Delta\sigma_n$ [50%] in MPa	314	332	168	176
$\Delta\sigma_n$ [95%] in MPa	290	305	162	165
SD	0.44	0.41	0.12	0.12

Table 6: Statistical analyses of fatigue test results for S690QL steel at VAL $R = -0.43$ in as-welded and HFMI treated conditions

	HFMI		As-welded	
	fixed slope	free slope	fixed slope	free slope
k :	5.6	7.4	4	3.95
$\Delta\sigma_n$ [50%] in MPa	950	965	590	590
$\Delta\sigma_n$ [95%] in MPa	825	860	547	546
SD	0.23	0.2	0.06	0.06

The degree of fatigue strength improvement by HFMI treatment is due to induced compressive residual stresses and to the reduced stress concentration factor. General observation for VAL is that higher stress levels may lead to a severe reduction of induced (beneficial) compressive residual stresses than at CAL [27]. For welds with AH36 as well as S690QL, the increase in fatigue strength at CAL by HFMI is similar when compared to the respective value for VAL at the region of $2 \times 10^6 < N_f < 2 \times 10^7$, Tables 7 and 9. However, there is almost no increase observed for AH36 steel in the low cycle fatigue region, namely at 2×10^5 where the SN lines merge, see Figure 10. On the contrary, the test results for S690QL show significant increase even at the low cycle fatigue region, see Figure 11.

When it comes to the overall improvement by additional consideration of VAL, Gassner-lines for as-welded and HFMI-treated conditions for both steel types are significantly above the respective Woehler-lines, Figures 10 and 11. Tables 8 - 10 present exceedance of Woehler-line by Gassner-line for AH36 and S690QL, respectively. These values would be smaller below the knee-points because of the flatter slopes of the Woehler-lines. The importance of these factors is that, for a given VAL spectrum and a required fatigue life, much higher fatigue strengths are allowed for a component subject to VAL than for one at CAL.

Table 7: Improvement by HFMI treatment for AH36

N_f	CAL (HFMI vs AW)	VAL (HFMI vs AW)	Overall (HFMI-VAL vs AW-CAL)
2×10^6	1.20	1.20	4.27
2×10^7	1.35	1.55	4.80

Table 8: Exceedance of the Woehler-line by the Gassner-line for AH36

N_f	AW (VAL vs CAL)	HFMI (VAL vs CAL)	Overall (HFMI-VAL vs AW-CAL)
2×10^6	3.57	3.55	4.27
2×10^7	3.10	3.55	4.80

Table 9: Improvement by HFMI-treatment for S690QL

N_f	CAL (HFMI vs AW)	VAL (HFMI vs AW)	Overall (HFMI-VAL vs AW-CAL)
2×10^6	1.87	1.61	5.65
2×10^7	2.10	2.08	6.34

Table 10: Exceedance of the Woehler-line by the Gassner-line for S690QL

N_f	AW (VAL vs CAL)	HFMI (VAL vs CAL)	Overall (HFMI-VAL vs AW-CAL)
2×10^6	3.51	3.03	5.65
2×10^7	3.05	3.03	6.34

3.4. *Fracture surface analysis*

Figure 12 shows the typical fracture surfaces of failed specimens tested at CAL for different load ranges in each condition. Cracks typically initiated from the centre in the case of as-welded specimens whereas initial cracks appeared close to on edge of the plate in the case of HFMI treatment.

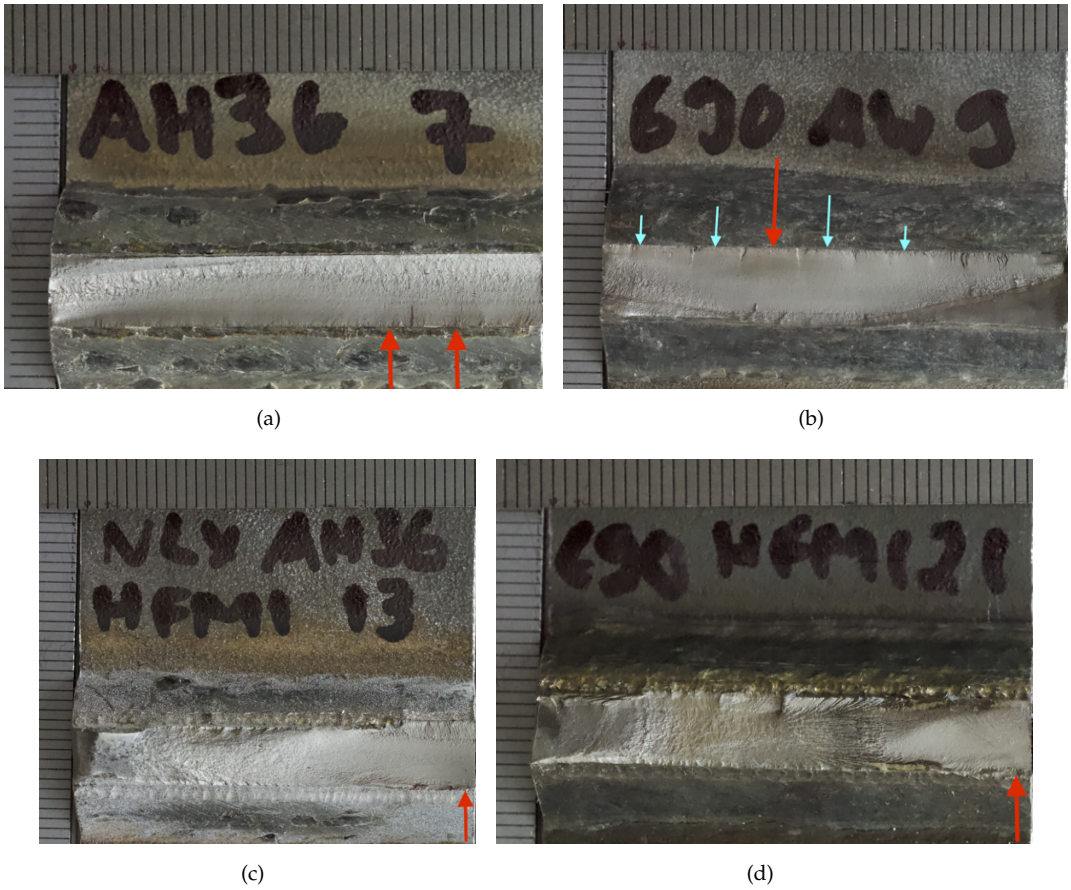

(a) (b) (c) (d)

Figure 12: Example sample failures for non-load carying specimens in both conditions: (a) Centre crack initiation of AH36-AW-7 at CAL with $\Delta\sigma_n = 190MPa$ and $R = -0.43$; (b) Centre crack initiation of S690QL-AW-9 at CAL with $\Delta\sigma_n = 262MPa$ and $R = -0.43$; (c) Edge crack initiation of AH36-HFMI-13 at CAL with $\Delta\sigma_n = 181MPa$ and $R = -0.43$; and, (d) Edge crack initiation of S690QL-HFMI-21 at CAL with $\Delta\sigma_n = 357MPa$ and $R = -0.43$.

The S690 specimen in the as-welded condition shows ratchet marks in the fracture surfaces, see Figure 12(b). Their presence indicates that there have been multiple crack initiation locations and the ratchet marks have formed as cracks on different failure planes coalesce. In this case, red arrow indicates the primary crack initiation location, deduced by the directions of the ratchet lines,

whereas blue arrows indicate the other crack initiation locations. Fewer ratchet marks were visible for the AH36 specimen in the as-welded condition, for example, the fracture surface in Figure 12(a) has one. Occurrence of ratchet marks under relatively low loads indicates the existence of severe stress concentrations in the weld [29]. On the other hand, there has been no ratchet marks observed in the HFMI-treated conditions of both steel grades.

Figure 13 shows an example investigation for the fracture surface analysis of a specimen subjected to the service loading. The observation was carried out by the scanning electron microscope. The studied sample was S690QL-HFMI-6, and it was tested at VAL with a maximum applied stress of 665 MPa which corresponds to the 80% of the material yield strength. This particular specimen was selected since the induced (beneficial) compressive stress state at the weld area may relax at this level of applied stress. Eventually, multiple crack initiation points along the weld groove could be observed, as in the case of the investigated fracture surface. Another important factor might be the introduced irregularities at the weld groove due to the impacts of the intenders. More specifically, a typical crack initiation point due to the impact is identified with a green area in Figure 13. The crack, at this point, was around 140 µm, which is visible from the magnified surfaces of 29 to 238 times and the growth pattern is shown with the red arrows in Figure 13.

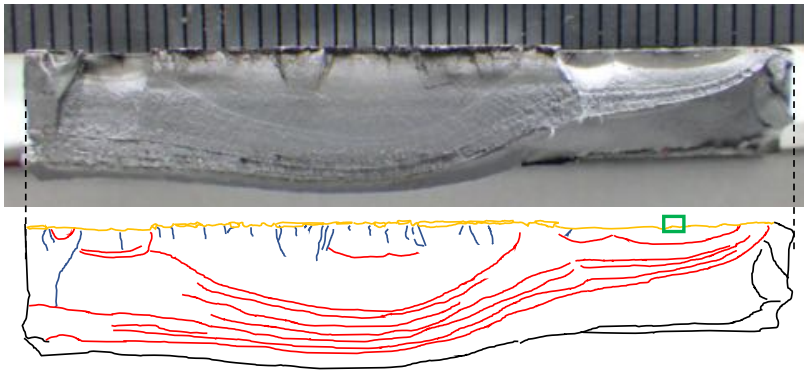

(a)

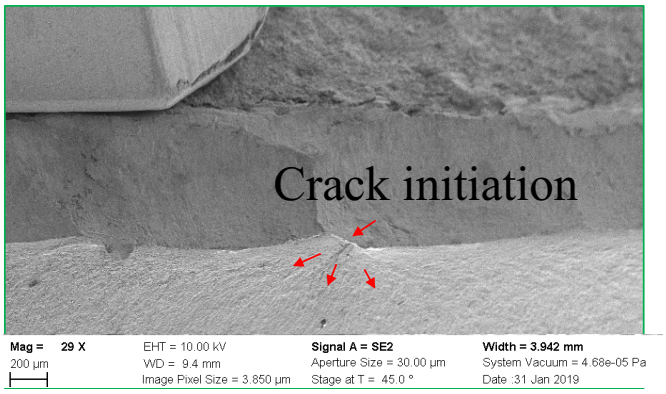

(b)

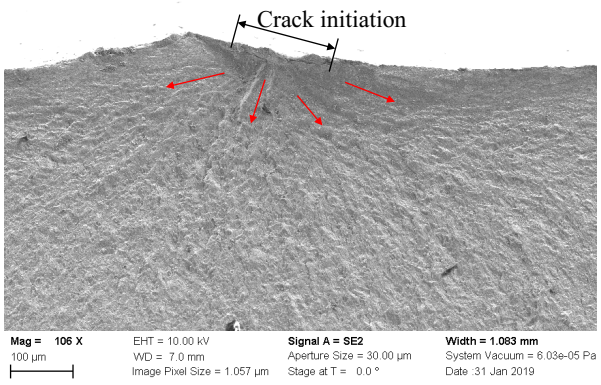

(c)

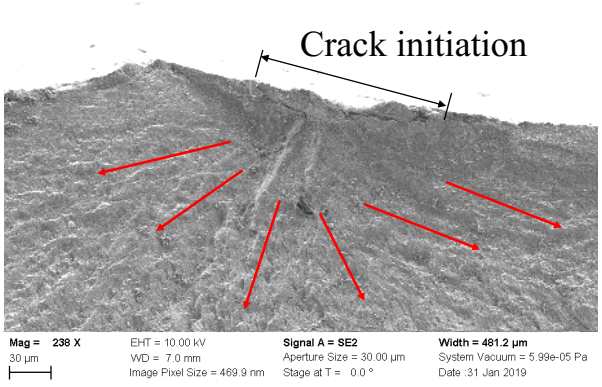

(d)

Figure 13: The SEM fractographs of S690QL-HFMI-6 subjected to VAL of $R = -0.43$ with $\Delta\sigma_{max} = 665MPa$, $\Delta\sigma_n = 951MPa$, and $N_f = 4788750Cycles$: (a) The development of the fatigue fracture surface; (b) 45 degrees magnified view of one of the crack initiation points at the weld toe; (c) Cross section view of the same crack; and, (d) Approximate length of 140 µm central crack.

3.5. Cumulative damage calculation

The accuracy of the linear damage accumulation hypothesis of Palmgren-Miner,

$$\sum(n/N)_i = D \tag{2}$$

with its modification according to Haibach [30], as considered in the IIW-Recommendations [3], was also analysed. The modification suggested by Haibach changes the slope of the Woehler-line after the knee point, with the slope of $k' = 2k - m$, with $m = 1.0$ for wrought material states and $m = 2.0$ for cast, weld and other non-homogenous material states.

In these calculations, failure was assumed to ideally occur at $D = D_{th} = 1.0$. On the contrary researchers observed that most of the failures occur before this proposed theoretical value [27] [30]. Thus, IIW recommended an allowable damage value of $D_{al} = 0.5$ for engineering assessment in order to be on the more safer side for a such load spectra.

Figures 14 and 15 present the calculated Gassner-lines for as-welded and HFMI-treated joints with AH36 and S690QL, respectively, according to Palmgren–Miner rule with the modification of Haibach. In these results, experimental Gassner-lines are compared with those of calculated for the theoretical and allowable damage sums, namely $D_{th} = 1.0$ and $D_{al} = 0.5$.

Tables 11 and 12 show the real damage sums at certain stress levels, where the real damage sum was calculated via

$$D_{real} = N_{exp}/N_{calc} \tag{3}$$

at $D_{th} = 1.0$.

The evaluated real damage sums are on the safe side for AH36 steels in the as-welded and HFMI treated conditions. For the S690QL steel, however, the approach for experimental values are in close agreement with the theoretical value of $D_{th} = 1.0$ for the HFMI condition. The values of the real damage sums are closer to the allowable value of $D_{th} = 0.5$ in the case of as-welded condition. Nevertheless it should be noted that the actual damage sums determined here might be dramatically different for other spectrum types and stress ratios.

Table 11: Real damage sums by comparison of experimental and calculated fatigue lives for AH36 in as-welded and HFMI-treated conditions

As-welded $\sigma_{an,k}$ = 47 MPa				HFMI $\sigma_{an,k}$ = 64 MPa			
σ_{an} in MPa	N_{calc} ($D_{th} = 1.0$)	N_{exp}	D_{real}	σ_{an} in MPa	N_{calc} ($D_{th} = 1.0$)	N_{exp}	D_{real}
100	6.15E+07	8.26E+07	1.34	300	3.90E+05	2.13E+06	5.47
200	3.85E+06	5.16E+06	1.34	400	1.16E+05	4.26E+05	3.69
250	1.58E+06	2.11E+06	1.34	500	5.77E+04	1.22E+05	2.12
400	2.40E+05	3.23E+05	1.34	600	2.08E+04	4.40E+04	2.12

Table 12: Real damage sums by comparison of experimental and calculated fatigue lives for S690QL in as-welded and HFMI treated conditions

As-welded $\sigma_{an,k}$ = 56 MPa				HFMI $\sigma_{an,k}$ = 118 MPa			
σ_{an} in MPa	N_{calc} ($D_{th} = 1.0$)	N_{exp}	D_{real}	σ_{an} in MPa	N_{calc} ($D_{th} = 1.0$)	N_{exp}	D_{real}
100	1.21E+08	8.26E+07	0.68	300	3.03E+07	2.62E+07	0.87
200	7.54E+06	5.16E+06	0.68	400	6.05E+06	5.24E+06	0.87
250	3.09E+06	2.11E+06	0.68	500	1.73E+06	1.50E+06	0.87
400	4.71E+05	3.23E+05	0.68	600	6.24E+05	5.41E+05	0.87

3.6. Residual stress measurements

The three main directions, longitudinal (LD), transverse (TD) and normal (ND), of the welding plates were measured for AH36 material due to the available limited beam time. A monochromatic

neutron beam with a wavelength of 1.74 was used. In the case of surface measurement, a $1 \times 1 \times 1mm^3$ gauge volume of irradiated material was characterised for measurements in the longitudinal direction of the weld. The measurements in the normal and cross directions were performed with a $1 \times 1 \times 10mm^3$ gauge volume of irradiated material, oriented in the longitudinal direction. For the depth measurements, a $2 \times 2 \times 2mm^3$ gauge volume of irradiated material was characterised for all directions of the weld. Stresses were measured in the middle of the centre line of the sample at three different layers. The measurements where made along a 24 mm path starting from the middle of the attachment and ending over the main plate. For both measurement directions, the results are shown in detail in Figure 16b.

As it can be seen from Figure 16a, there is significant variation in depth residual stress measured in the longitudinal direction. Tensile residual stress state was observed at the weld toe region in the as-welded condition whereas compressive residual stress state was found in HFMI-treated welds due to the treatment at the near surface measurements. In Figure 16b this region corresponds to the distance from 6 to 10 mm in the horizontal axis, namely in x-axis. Moreover, tensile stresses reached up to 400 MPa around the weld root. This is expected since the maximum value is close to smaller than the material yield strength of 423 MPa. On the other hand, in depth measurements at the middle of the specimen showed different residual stress characteristic. The behaviour of compressive residual stresses was shifted to the tensile residual stresses close to the weld root following the HFMI treatment.

There may be issues regarding measuring the near-surface residual stresses by the neutron diffraction method since the gauge volume may be partially immersed at the surface. The peak shifts may result in a pseudo strain deviating the centre of the peak from its actual position owing to non-existing strain component and therefore, spurious readings of strain can be recorded. In this study, to avoid this, the obtained data was treated with a mathematical method developed by Thilo [31]. First, the pseudo peak shift was determined experimentally by subtracting the entrance and exit curve considering twice measurement from front and back sides. Then the mathematical model was applied, refining beam dimensions and wavelength distribution. The used model takes into account curved surfaces and allows precise stress determination as close as 40 micrometres below the surface. In this study the near surface measurements were performed at a depth of 0.02 mm.

4. Conclusions

In this study, fatigue testing of transverse non-load carrying specimens at constant and variable amplitude loadings at a stress ratio of $R = -0.43$ was performed. Additional investigations on the specimen geometry, residual stress state, as well as microstructural and hardness measurements were also carried out.

Based on the experimental program on the welded specimens, which have been manufactured from 6 mm thick plates of the high-strength steel of AH36 and S690QL grades, the following conclusions can be drawn:

- The analyses show that the recommended and best-fit slopes are in close agreement for as-welded joints for both variable and constant amplitude loadings of $R = -0.43$. In the case of HFMI-treated welds, the best-fit slopes are larger than the recommended value, except for the tests at constant amplitude loading for $R = -0.43$.
- For the welded joints of AH36 and S690QL steel grades, the improvement factors by HFMI treatment at constant amplitude loading is similar when compared to the respective value at variable amplitude loading in the high cycle fatigue region. On the other hand, severe relaxation of compressive residual stresses at the low cycle fatigue region for AH36 steel grade

may have diminished the beneficial treatment effects. As for the resulting improvement by including the effects of variable amplitude loading, Gassner-lines are found to be significantly above the respective Woehler-lines for as-welded and HFMI-treated joints of both steel grades.

- For the given VAL spectrum, much higher fatigue strengths can be expected for a component subject to VAL than that of CAL.
- The calculated real damage sums are on the safe side for AH36 steels in the as-welded and HFMI treated conditions. For the S690QL steel, the experimental damage values are in close agreement with the theoretical damage value of 1.0 for the HFMI condition and damage values are closer to the allowable value of 0.5 in the case of as-welded condition.
- In depth residual stress measurements by neutrons have shown that the application of HFMI treatment has shifted the tensile residual stresses from the weld toe to the weld root area.
- The angular misalignments of specimens varies between 0 and 1 degrees, resulting in stress magnification factor k_m between 1 and 1.4. The mean value of k_m factor is slightly lower for the HFMI-treated welded joints than that of as-welded joints. Absolute maximum value is, however, similar for both HFMI-treated and as-welded states.
- The hardness values for most of the samples are found to be in the acceptable range with peak values in the HAZ and slightly higher hardness in the weld material than in the base material. Higher hardness values are observed in the base material of the HFMI-treated AH36 material and high peak hardness in the HAZ of one of the welds in the same sample. This might be due to cyclic hardening occurred due to the load history.
- The hardness values for the base and weld materials are higher for the S690QL grade than that of the AH36 grade, however the peak hardness in the HAZ is not much different between the two steel grades.
- The effect of the HFMI treatment is visible from the macrographs. The HFMI-treated specimen for AH36 steel grade has concave geometry and sharp lips/corners probably introduced by the HFMI treatment. Similar irregularities are not visible for the specimen manufactured from S690QL steel grade for the treated or as-welded conditions.

The results presented in this paper cannot be generalised as different material behaviour may be observed from the interaction of weld geometry, local stress concentration and residual stress state, spectrum shape and finally, loading history. Nonetheless, cumulative damage calculations from the IIW recommendations can be applied satisfyingly.

Acknowledgements

Partially support of this work was provided under the European Project **Hi-Life** of Horizon 2020 with the Grant Agreement ID 702233: *Damage mechanism of High Frequency Mechanical Impact (HFMI) Treated Welded Structures under Service Loading to Increase the Fatigue Life for Lightweight Design*.

The authors would like to thank Paul Lefevre from SONATS for carrying out the post weld treatment, Pauli Lehto from Aalto University for sample preparation, etching, microstructural imaging and related data processing and analysis of the hardness measurements, Oskar Siljama for helping the 3D geometry measurements, Susanna Hurme and Yuki Ono for helping with the fatigue testing and fracture surface investigations at Aalto University and EPFL, respectively, and Meyer Turku Shipyard for providing the welded steel plates.

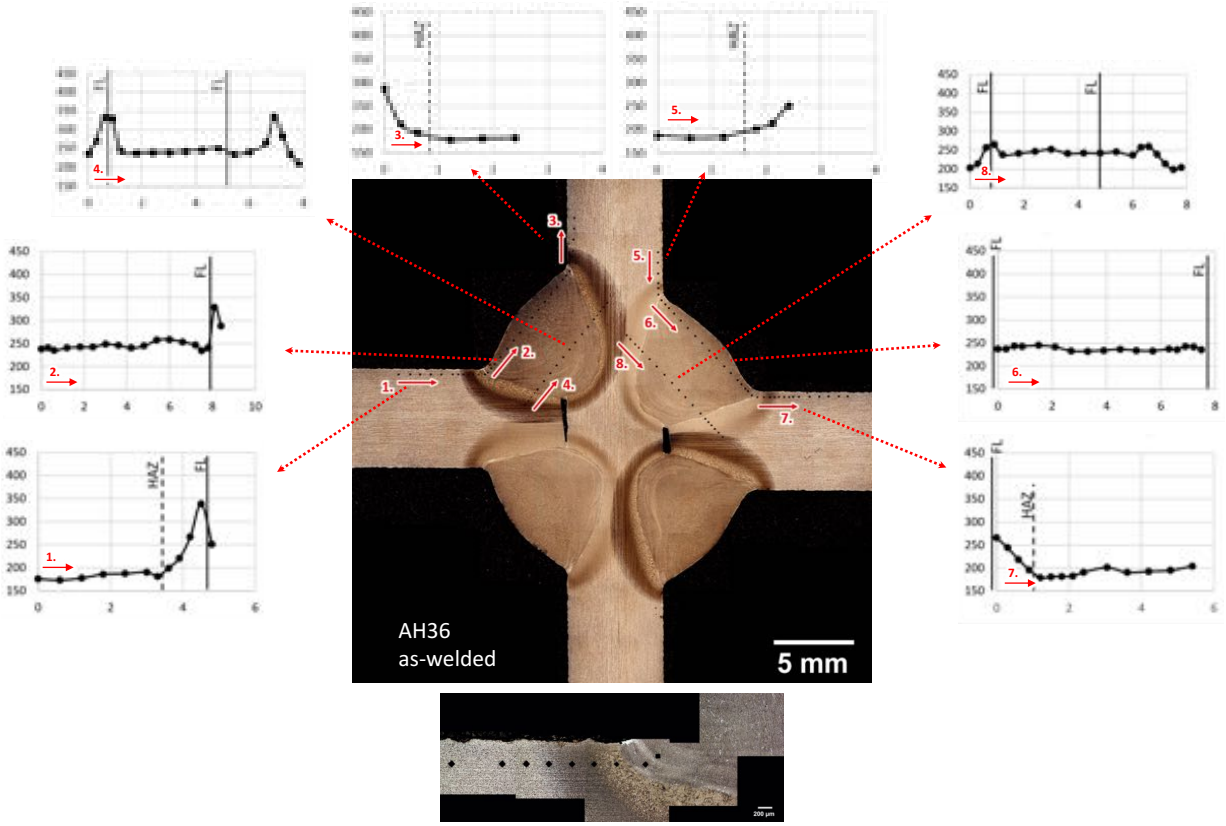

(a) As-welded condition (AH36-AW-20)

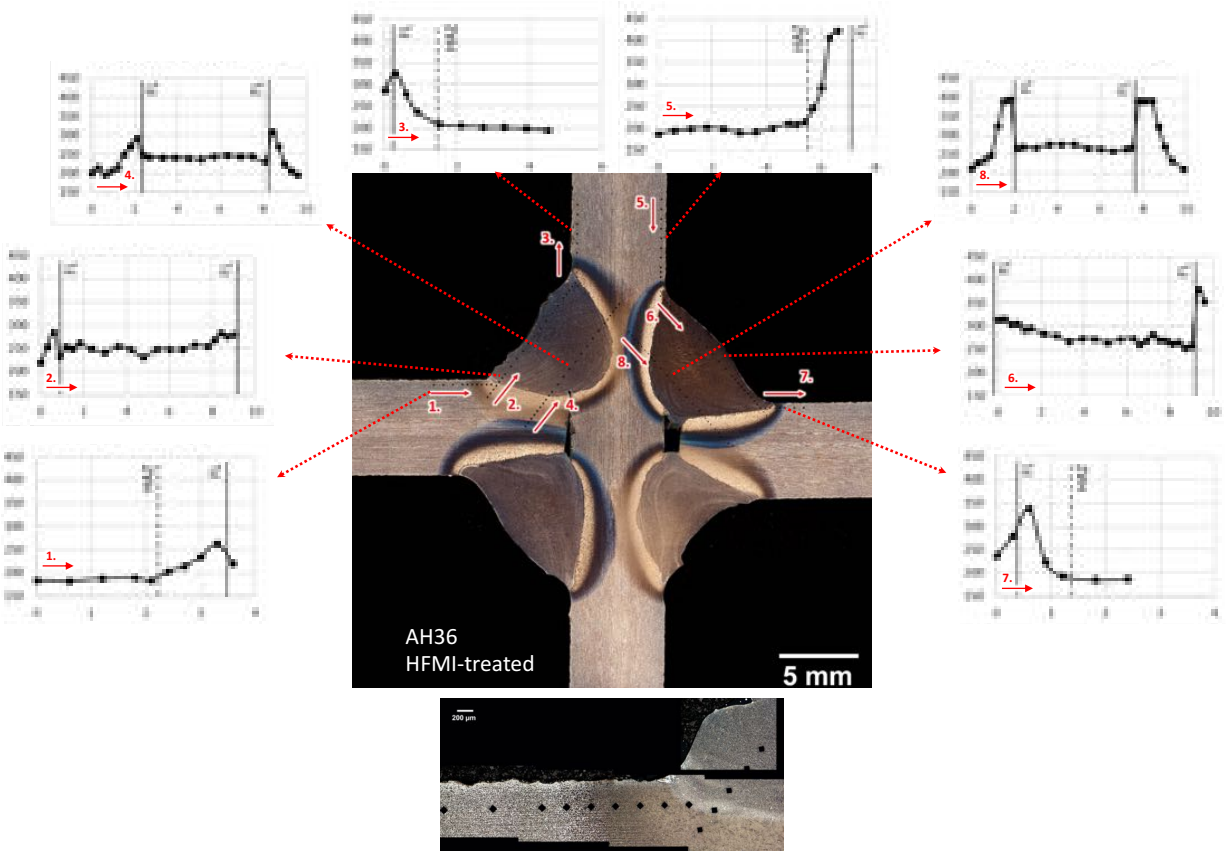

(b) HFMI-treated condition (AH36-HFMI-20)

Figure 8: Macrosection and hardness values of AH36 steel in as-welded and HFMI treated condition, with 100x magnification micrograph for the weld on top-left side. Locations of fusion line (FL) and heat-affected zone (HAZ) are depicted. The numbers indicate the measurement locations and directions. Microhardness was measured using an instrumented Vickers hardness test device and load of 1000 gf equivalent to HV1.

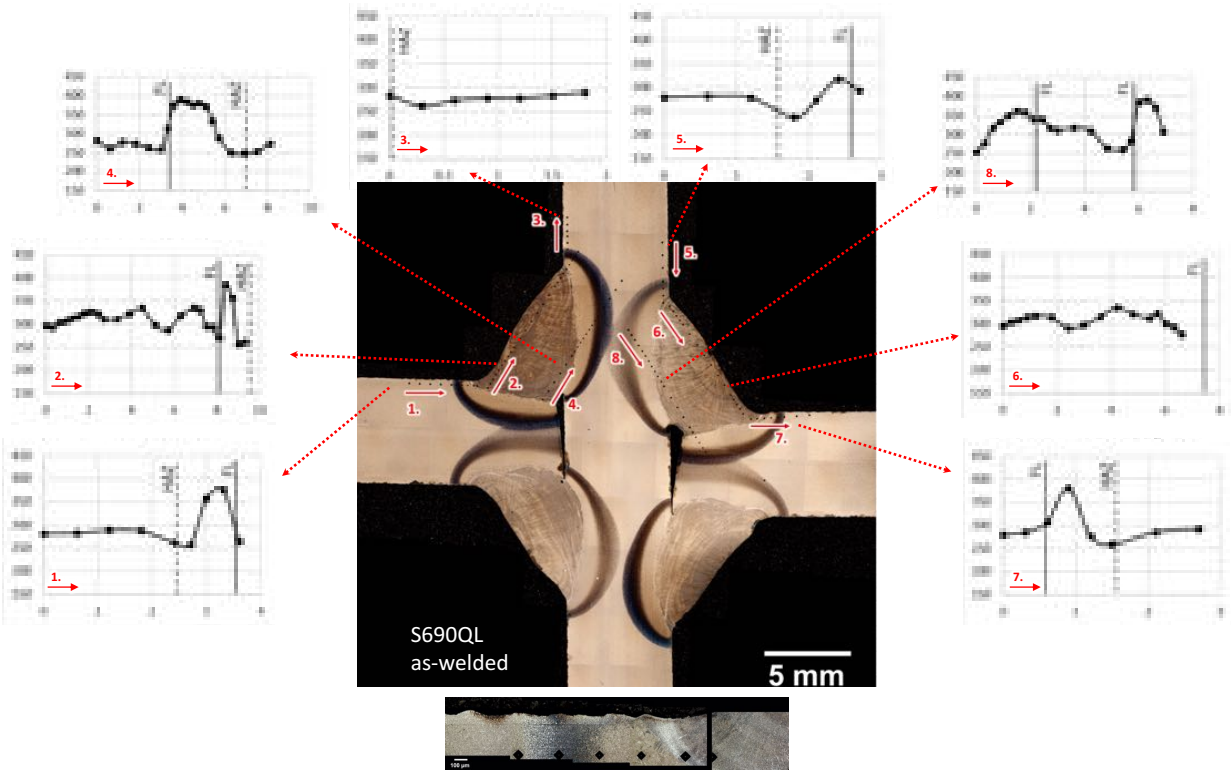

(a) As-welded condition (S690QL-AW-21)

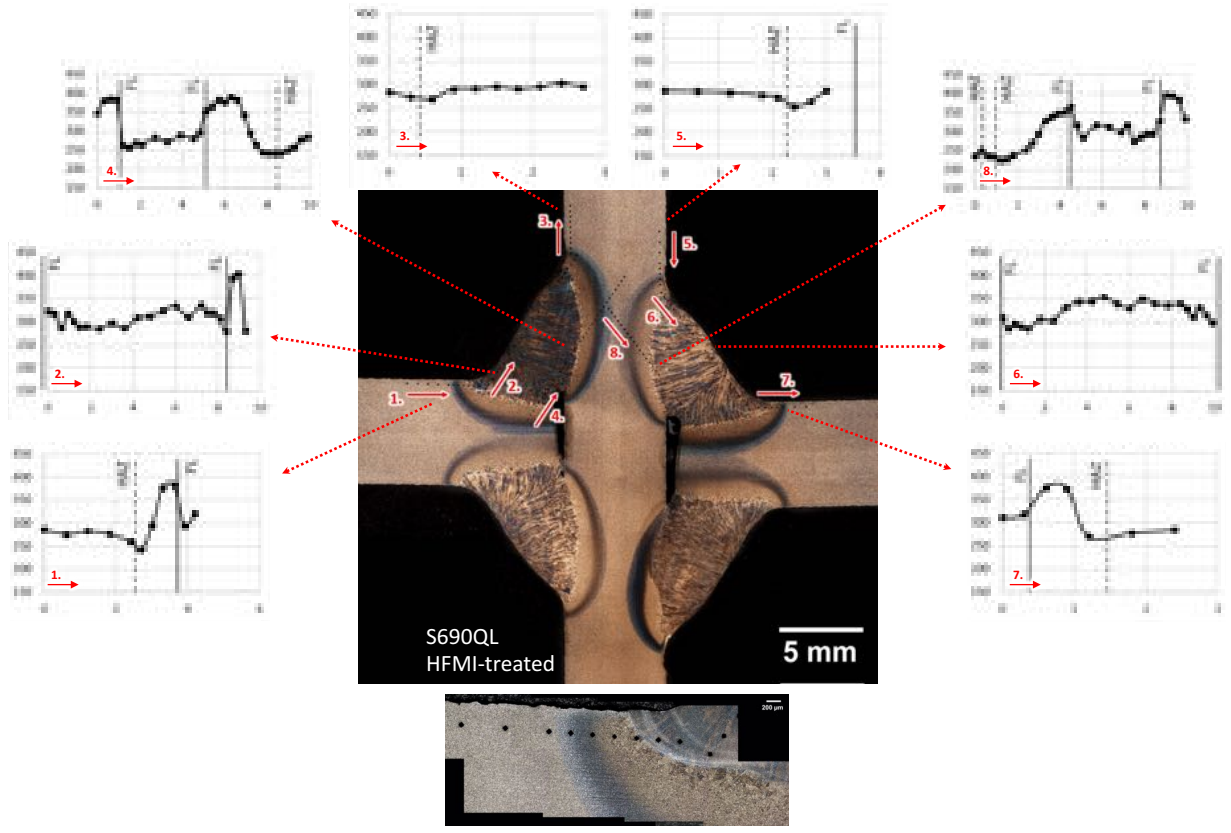

(b) HFMI-treated condition (S690QL-HFMI-17)

Figure 9: Macrosection and hardness values of S690QL in as-welded and HFMI treated condition, with 100x magnification micrograph for the weld on top-left side. Locations of fusion line (FL) and heat-affected zone (HAZ) are depicted. The numbers indicate the measurement locations and directions. Microhardness was measured using an instrumented Vickers hardness test device and load of 1000 gf equivalent to HV1.

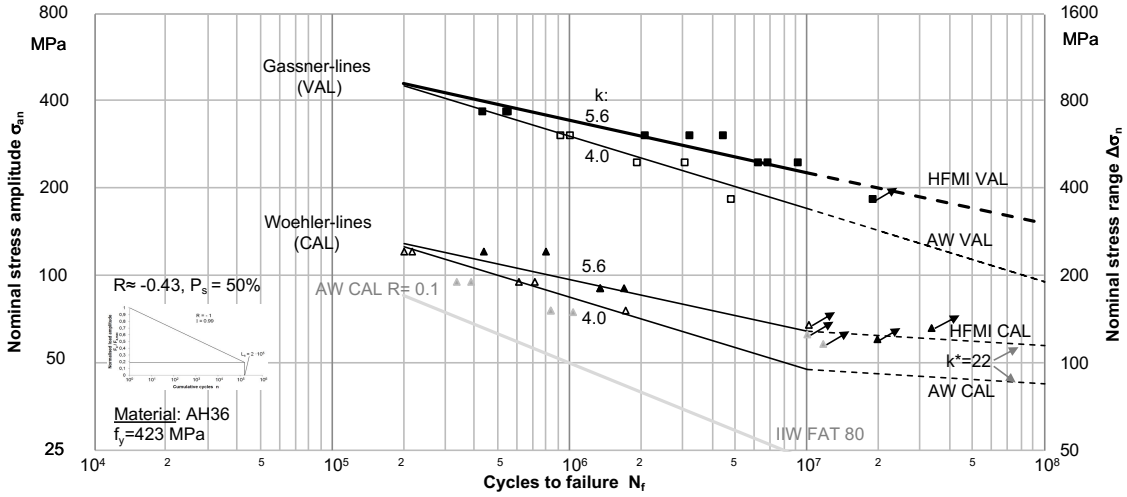

Figure 10: Fatigue test results of AH36 steel in as-welded and HFMI-treated conditions.

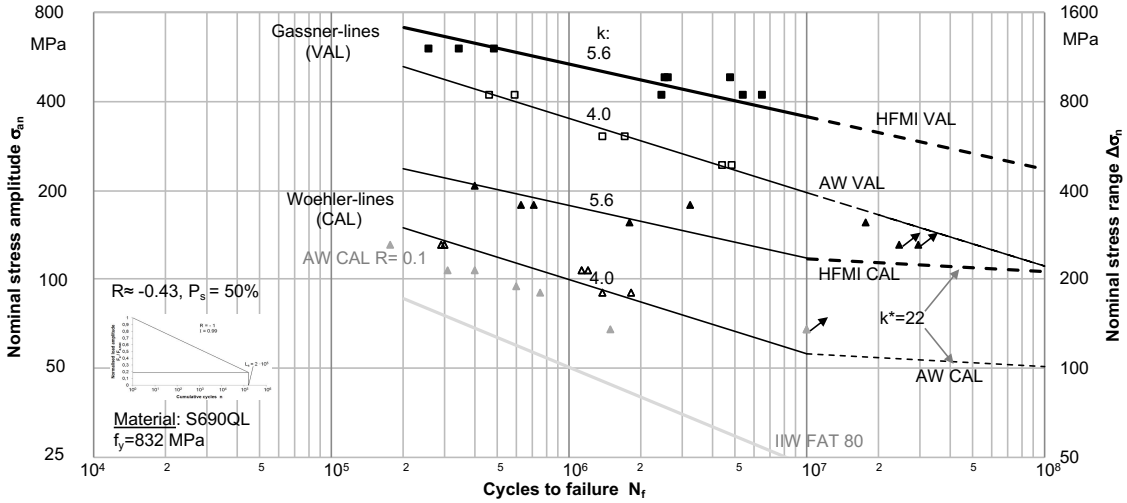

Figure 11: Fatigue test results of S690QL steel in as-welded and HFMI treated conditions.

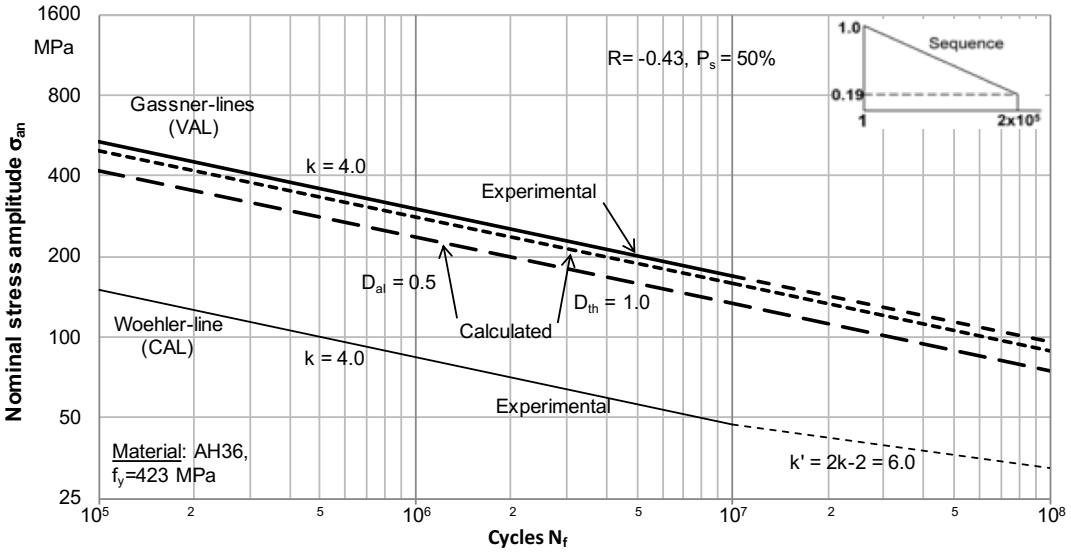

(a) As-welded condition

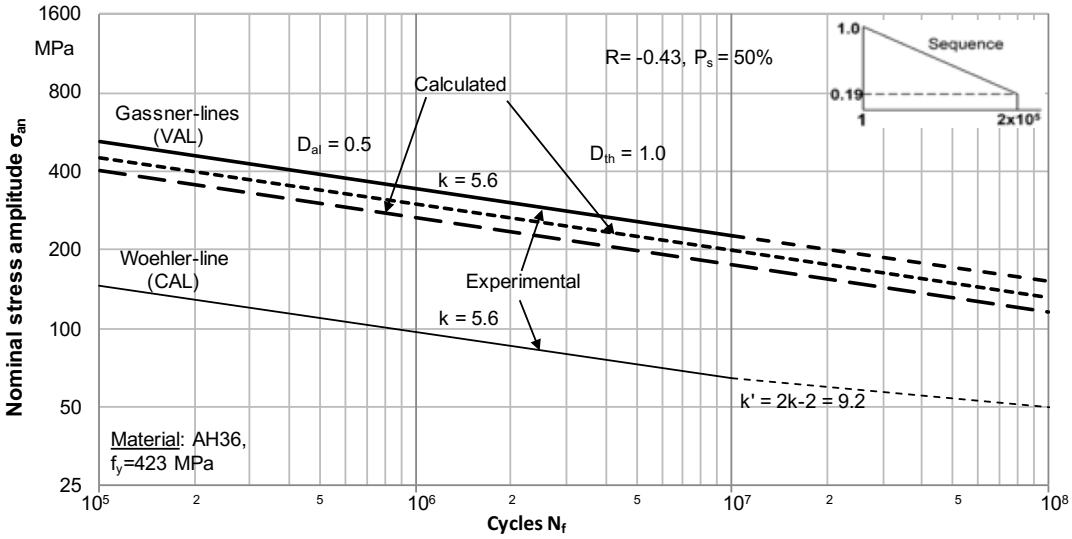

(b) HFMI-treated condition

Figure 14: Calculated Gassner-lines for as-welded and HFMI-treated joints with AH36 according to Palmgren–Miner rule with the modification of Haibach

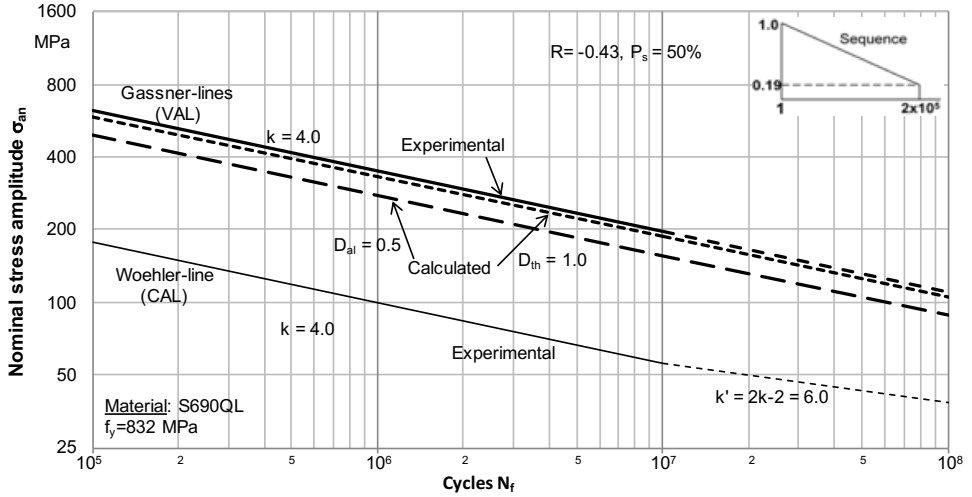

(a) As-welded condition

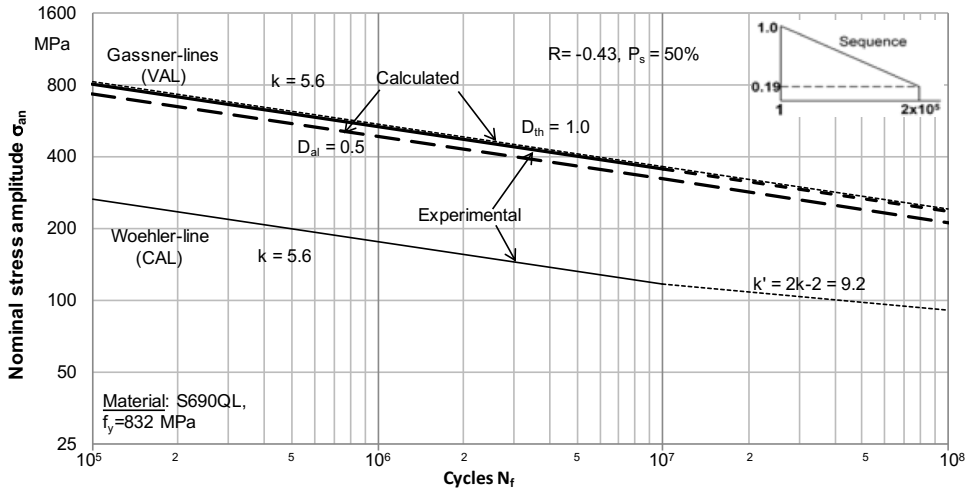

(b) HFMI-treated condition

Figure 15: Calculated Gassner-lines for as-welded and HFMI-treated joints with S690QL according to Palmgren–Miner rule with the modification of Haibach

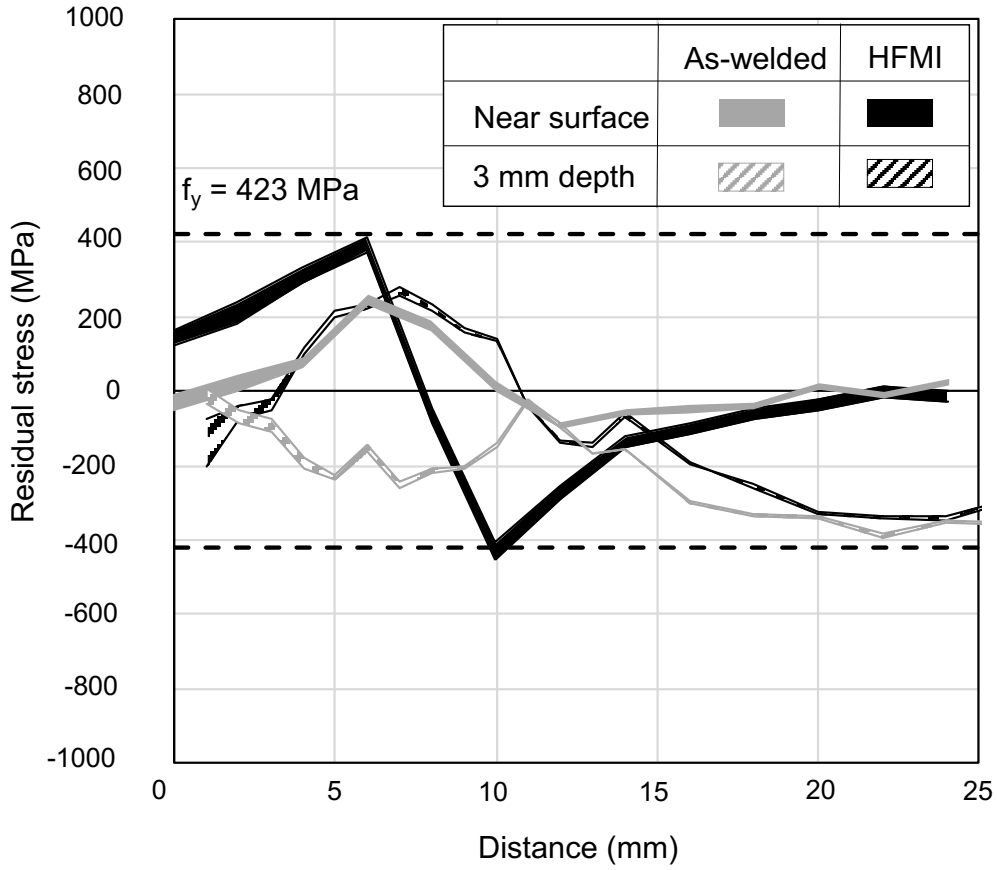

(a) Residual stress distribution of welded specimen of AH36 steel before and after the treatment.

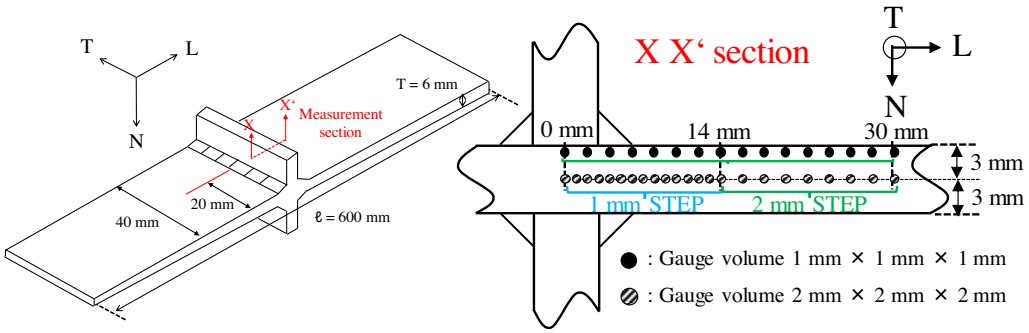

(b) Detail description of the measurement points

Figure 16: Residual stress distribution of transverse attachments around the weld toe region at near the surface and 3 mm in depth. Nondestructive measurements were carried out by the neutron diffraction facilities.

References

[1] T. R. Gurney, Fatigue of Welded Structures,Cambridge University Press, 1968.

[2] K. Kirkhope, R. Bell, L. Caron, R. Basu, K.-T. Ma, Weld detail fatigue life improvement techniques. part 1: review, Marine Structures 12 (6) (1999) 447 – 474. doi:https://doi.org/10.1016/S0951-8339(99)00013-1.
URL http://www.sciencedirect.com/science/article/pii/S0951833999000131

[3] A. F. Hobbacher, IIW recommendations for fatigue design of welded joints and components, springer international publishing, second edition, 978-3-319-23757-2 (2015).

[4] H. C. Yildirim, G. B. Marquis, Fatigue strength improvement factors for high strength steel welded joints treated by high frequency mechanical impact, International Journal of Fatigue 44 (2012) 168 – 176. doi:https://doi.org/10.1016/j.ijfatigue.2012.05.002.
URL http://www.sciencedirect.com/science/article/pii/S0142112312001648

[5] H. Yıldırım, G. Marquis, C. Sonsino, Lightweight design with welded high-frequency mechanical impact (hfmi) treated high-strength steel joints from s700 under constant and variable amplitude loadings, International Journal of Fatigue 91 (2016) 466 – 474, variable Amplitude Loading. doi:https://doi.org/10.1016/j.ijfatigue.2015.11.009.
URL http://www.sciencedirect.com/science/article/pii/S0142112315003990

[6] H. C. Yıldırım, G. B. Marquis, Fatigue design of axially-loaded high frequency mechanical impact treated welds by the effective notch stress method, Materials and Design 58 (2014) 543 – 550. doi:https://doi.org/10.1016/j.matdes.2014.02.001.
URL http://www.sciencedirect.com/science/article/pii/S0261306914001046

[7] X. Zhao, D. Wang, L. Huo, Analysis of the s-n curves of welded joints enhanced by ultrasonic peening treatment, Materials and Design 32 (1) (2011) 88–96, cited By 49. doi:10.1016/j.matdes.2010.06.030.
URL https://www.scopus.com/inward/record.uri?eid=2-s2.0-77956171437&doi=10.1016%2fj.matdes.2010.06.030&partnerID=40&md5=f3883e26fc784b05c52a58c05815c315

[8] G. B. Marquis, E. Mikkola, H. C. Yıldırım, Z. Barsoum, Fatigue strength improvement of steel structures by high-frequency mechanical impact: proposed fatigue assessment guidelines, Welding in the World 57 (6) (2013) 803–822. doi:10.1007/s40194-013-0075-x.
URL http://dx.doi.org/10.1007/s40194-013-0075-x

[9] E. Mikkola, H. Remes, Allowable stresses in high-frequency mechanical impact (hfmi)-treated joints subjected to variable amplitude loading, Welding in the World 61 (1) (2017) 125–138. doi:10.1007/s40194-016-0400-2.
URL https://doi.org/10.1007/s40194-016-0400-2

[10] H. C. Yıldırım, Recent results on fatigue strength improvement of high-strength steel welded joints, International Journal of Fatigue 101 (2017) 408 – 420, fatigue Assessment of Welded Joints by Modern Concepts. doi:https://doi.org/10.1016/j.ijfatigue.2016.10.026.
URL http://www.sciencedirect.com/science/article/pii/S0142112316303553

[11] C. Revilla-Gomez, J.-Y. Buffiere, C. Verdu, C. Peyrac, L. Daflon, F. Lefebvre, Assessment of the surface hardening effects from hammer peening on high strength steel, Procedia Engineering 66 (2013) 150 – 160, fatigue Design 2013, International Conference Proceedings. doi:https://doi.org/10.1016/j.proeng.2013.12.070.
URL http://www.sciencedirect.com/science/article/pii/S1877705813019036

[12] I. Weich, T. Ummenhofer, T. Nitschke-Pagel, K. Dilger, H. Eslami Chalandar, Fatigue behaviour of welded high-strength steels after high frequency mechanical post-weld treatments, Welding in the World 53 (11) (2009) R322–R332. doi:10.1007/BF03263475.
URL https://doi.org/10.1007/BF03263475

[13] G. Le Quilliec, H.-P. Lieurade, M. Bousseau, M. Drissi-Habti, G. Inglebert, P. Macquet, L. Jubin, Fatigue behaviour of welded joints treated by high frequency hammer peening: Part i , experimental study., 64th Annual Assembly International Conference of the International Institute of Welding (IIW 2011), Jul 2011, Chennai, India.
URL https://www.archives-ouvertes.fr/hal-01332675/document

[14] M. Malaki, H. Ding, A review of ultrasonic peening treatment, Materials and Design 87 (2015) 1072 – 1086. doi:https://doi.org/10.1016/j.matdes.2015.08.102.
URL http://www.sciencedirect.com/science/article/pii/S0264127515303518

[15] M. G. Khurshid M, Barsoum Z, Behavior of Compressive Residual Stresses in High Strength Steel Welds Induced by High Frequency Mechanical Impact Treatment. ASME. Pressure Vessels and Piping Conference, Volume 5: High-Pressure Technology; ASME NDE Division; Rudy Scavuzzo Student Paper Symposium:V005T11A001., 2013.

[16] E. Mikkola, G. Marquis, P. Lehto, H. Remes, H. Hänninen, Material characterization of high-frequency mechanical impact (hfmi)-treated high-strength steel, Materials and Design 89 (2016) 205 – 214. doi:https://doi.org/10.1016/j.matdes.2015.10.001.
URL http://www.sciencedirect.com/science/article/pii/S0264127515305797

[17] E. Mikkola, H. Remes, G. Marquis, A finite element study on residual stress stability and fatigue damage in high-frequency mechanical impact (hfmi)-treated welded joint, International Journal of Fatigue 94 (2017) 16 – 29. doi:https://doi.org/10.1016/j.ijfatigue.2016.09.009.
URL http://www.sciencedirect.com/science/article/pii/S0142112316302821

[18] J. Schubnell, P. Pontner, R. Wimpory, M. Farajian, V. Schulze, The influence of work hardening and residual stresses on the fatigue behavior of high frequency mechanical impact treated surface layers, International Journal of Fatigue 134 (2020) 105450. doi:https://doi.org/10.1016/j.ijfatigue.2019.105450.
URL http://www.sciencedirect.com/science/article/pii/S0142112319305547

[19] SSAB, AH36 technical data sheet, Raahe Steel Works, 2017.

[20] SSAB, S690QL technical data sheet, Raahe Steel Works, 2017.

[21] VDI/VDE, 2634 Part 3, Optical 3D-measuring systems, Multiple view systems based on area scanning, Verein Deutscher Ingenieure, 2008.

[22] H. C. Yildirim, G. B. Marquis, A round robin study of high-frequency mechanical impact (hfmi)-treated welded joints subjected to variable amplitude loading, Welding in the World 57 (3) (2013) 437–447. doi:10.1007/s40194-013-0045-3.
URL https://doi.org/10.1007/s40194-013-0045-3

[23] Stress-spec materials science diffractometer, https://www.mlz-garching.de/stress-spec, accessed: 2020-02-20.

[24] Strain analyser for engineering applications, https://www.ill.eu/users/instruments/instruments-list/salsa/description/instrument-layout/, accessed: 2020-02-20.

[25] J. P. Nobre, A. C. Batista, J. R. Kornmeier, J. D. Costa, A. Loureiro, J. S. Jesus, Neutron and x-ray diffraction residual stress measurements in aluminium alloys mig welded t-joints after friction stir processing, in: Residual Stresses IX, Vol. 996 of Advanced Materials Research, Trans Tech Publications, 2014, pp. 439–444. doi:10.4028/www.scientific.net/AMR.996.439.

[26] DNV-GL, Rules for clarification, Part 2 Materials and Welding, Chapter 4 Fabrication and Testing, Edition July 2018.

[27] C. Sonsino, Course of sn-curves especially in the high-cycle fatigue regime with regard to component design and safety, International Journal of Fatigue 29 (12) (2007) 2246 – 2258. doi:https://doi.org/10.1016/j.ijfatigue.2006.11.015.
URL http://www.sciencedirect.com/science/article/pii/S014211230600346X

[28] H. C. Yıldırım, G. Marquis, C. M. Sonsino, Lightweight potential of welded high-strength steel joints from s700 under constant and variable amplitude loading by high-frequency mechanical impact (hfmi) treatment, Procedia Engineering 101 (2015) 467 – 475, 3rd International Conference on Material and Component Performance under Variable Amplitude Loading, VAL 2015. doi:https://doi.org/10.1016/j.proeng.2015.02.056.
URL http://www.sciencedirect.com/science/article/pii/S1877705815006542

[29] N. Sachs, Understanding the surface features of fatigue fractures: How they describe the failure cause and the failure history, Fail. Anal. and Preven 5 (2005) 11 – 15.

[30] E. Haibach, Betriebsfestigkeit - Verfahren und Daten zur Berechnung (Structural durability - Methods and data for calculation). 2nd ed. Dusseldorf: VDI-Verlag; .

[31] T. Pirling, Precise analysis of near surface neutron strain imaging measurements, Procedia Engineering 10 (2011) 2147 – 2152, 11th International Conference on the Mechanical Behavior of Materials (ICM11). doi:https://doi.org/10.1016/j.proeng.2011.04.355.
URL http://www.sciencedirect.com/science/article/pii/S1877705811005431

Appendices

A. Transverse non-load carrying attachment

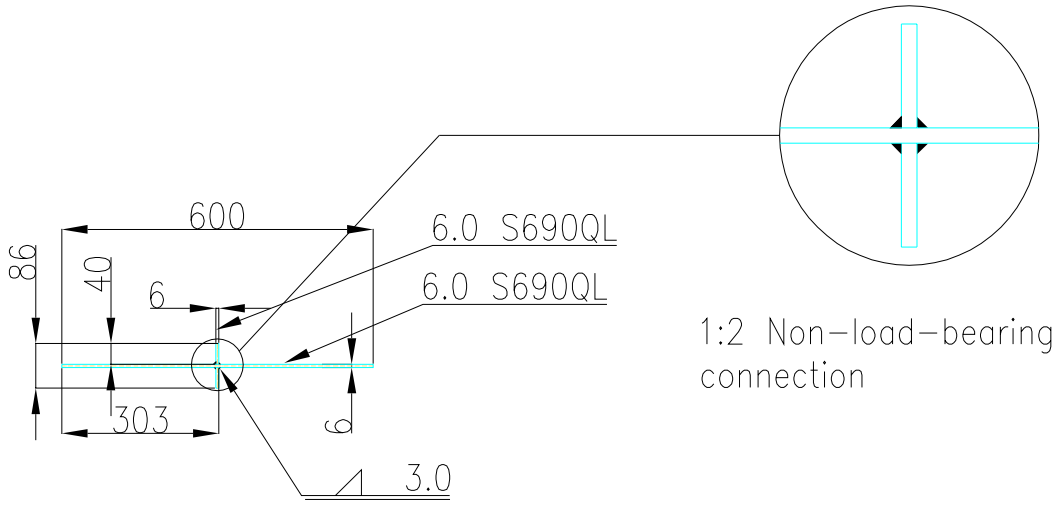

Figure 17: Technical drawing of transverse non-load carrying attachment

B. Fatigue test results of non-load carrying transverse specimens

Table 13: Fatigue test results of non-load carrying transverse specimens manufactured from AH36 steels in as-welded and HFMI treated conditions.

No	Condition	Inst	Material	Loading	R	$\Delta\sigma$ [MPa]	σ_{amp} [MPa]	σ_{mean} [MPa]	N_f	Crack initiation point
1	AW	Aalto	AH36	CA1, $\Delta\sigma$ = 153 MPa, (0.4*fy)	0,1	153	77	94	827502	Centre, weld toe failure
2	AW	Aalto	AH36	CA2, $\Delta\sigma$ = 117 MPa, (0.3*fy)	0,1	117	59	72	11700000	Interrupted
3	AW	Aalto	AH36	CA3, $\Delta\sigma$ = 190 MPa, (0.5*fy)	0,1	190	95	116	334910	Centre, weld toe failure
4	AW	Aalto	AH36	CA1, $\Delta\sigma$ = 153 MPa, (0.4*fy)	0,1	153	77	94	837466	Centre, weld toe failure
5	AW	Aalto	AH36	CA2, $\Delta\sigma$ = 126 MPa, (0.3*fy)	0,01	125	63	64	10052008	Interrupted
6	AW	Aalto	AH36	CA3, $\Delta\sigma$ = 190 MPa, (0.5*fy)	0,1	190	95	116	383736	Centre, weld toe failure
7	AW	Aalto	AH36	CA1, $\Delta\sigma$ = 190 MPa, (0.3*fy)	-0,43	190	95	38	608805	Centre, weld toe failure
8	AW	Aalto	AH36	CA2, $\Delta\sigma$ = 243 MPa, (0.4*fy)	-0,43	243	122	48	201094	Centre, weld toe failure
9	AW	Aalto	AH36	CA3, $\Delta\sigma$ = 153 MPa, (0.25*fy)	-0,43	153	77	30	1723400	Centre, weld toe failure
10	AW	Aalto	AH36	CA4, $\Delta\sigma$ = 136 MPa, (0.225*fy)	-0,43	136	68	27	10122344	Interrupted
11	AW	Aalto	AH36	CA2, $\Delta\sigma$ = 243 MPa, (0.4*fy)	-0,43	243	122	48	217785	Centre, weld toe failure
12	AW	Aalto	AH36	CA1, $\Delta\sigma$ = 190 MPa, (0.3*fy)	-0,43	190	95	38	710346	Centre, weld toe failure
13	AW	EPFL	AH36	VA1, σ_{max}= 338 MPa, (0.8*fy)	-0,43	483	242	96	1955016	Centre, weld toe failure
16	AW	EPFL	AH36	VA0, σ_{max}= 423 Mpa (1.0*fy)	-0,43	605	302	121	1021112	Centre, weld toe failure
17	AW	EPFL	AH36	VA1, σ_{max}= 338 MPa, (0.8*fy)	-0,43	483	242	96	3087889	Centre, weld toe failure
18	AW	EPFL	AH36	VA0, σ_{max}= 423 Mpa (1.0*fy)	-0,43	605	302	121	931610	Edge, weld toe failure
19	AW	EPFL	AH36	CA5, $\Delta\sigma$ = 150 Mpa, (0.39*fy)	0,1	150	75	92	1041214	Edge, weld toe failure
1	HFMI	EPFL	AH36	VA1, σ_{max}= 338 MPa, (0.8*fy)	-0,43	483	242	96	9210750	Edge, weld toe failure
2	HFMI	EPFL	AH36	VA2, σ_{max}= 423 Mpa (1.0*fy)	-0,43	605	302	121	4473000	Edge, weld toe failure
3	HFMI	EPFL	AH36	VA3, σ_{max}= 254 MPa, (0.6*fy)	-0,43	363	182	72	19120500	Interruptted
4	HFMI	EPFL	AH36	VA2, σ_{max}= 423 MPa, (1.0*fy)	-0,43	605	302	121	3221250	Edge, weld toe failure
5	HFMI	EPFL	AH36	VA1, σ_{max}= 338 MPa, (0.8*fy)	-0,43	483	242	96	6921750	Edge, weld toe failure
6	HFMI	EPFL	AH36	VA0, σ_{max}= 508 MPa, (1.2*fy)	-0,43	726	363	145	551250	Edge, weld toe failure
7	HFMI	EPFL	AH36	VA1, σ_{max}= 338 MPa, (0.8*fy)	-0,43	483	242	96	6255000	Edge, weld toe failure
8	HFMI	EPFL	AH36	VA2, σ_{max}= 423 Mpa (1.0*fy)	-0,43	605	302	121	2092500	Edge, weld toe failure
9	HFMI	EPFL	AH36	VA3, σ_{max}= 254 MPa, (0.7*fy)	-0,43	423	212	84	5584500	Edge, Weld toe failure
10	HFMI	EPFL	AH36	VA0, σ_{max}= 508 MPa, (1.2*fy)	-0,43	726	363	145	560250	Edge, weld toe failure
12	HFMI	Aalto	AH36	CA1, $\Delta\sigma$ = 242 MPa, (0.4*fy)	-0,43	242	121	48	798406	Edge, weld toe failure
13	HFMI	Aalto	AH36	CA2, $\Delta\sigma$ = 181 MPa, (0.3*fy)	-0,43	181	91	36	1346563	Edge, weld toe failure
14	HFMI	EPFL	AH36	VA0, σ_{max}= 508 MPa, (1.2*fy)	-0,43	726	363	145	435750	Edge, weld toe failure
15	HFMI	Aalto	AH36	CA1, $\Delta\sigma$ = 242 MPa, (0.4*fy)	-0,43	242	121	48	433673	Edge, weld toe failure
16	HFMI	Aalto	AH36	CA2, $\Delta\sigma$ = 181 MPa, (0.3*fy)	-0,43	181	91	36	1351325	Edge, weld toe failure
17	HFMI	EPFL	AH36	CA3, $\Delta\sigma$ = 133 MPa, (0.22*fy)	-0,43	133	67	27	33602671	Interrupted
19	HFMI	Aalto	AH36	CA2, $\Delta\sigma$ = 181 MPa, (0.3*fy)	-0,43	181	91	36	1695096	Edge, weld toe failure
20	HFMI	Aalto	AH36	CA3, $\Delta\sigma$ = 133 MPa, (0.2*fy)	-0,43	121	61	24	19848784	Interrupted

Table 14: Fatigue test results of non-load carrying transverse specimens manufactured from S690QL steels in as-welded and HFMI treated conditions.

No	Condition	Inst	Material	Loading	R	$\Delta\sigma$ [MPa]	σ_{amp} [MPa]	σ_{mean} [MPa]	N_f	Crack initiation point
1	AW	Aalto	S690QL	CA1, $\Delta\sigma$ = 262 MPa, (0.35*fy)	0,1	262	131	160	177516	Centre, weld toe failure
2	AW	Aalto	S690QL	CA2, $\Delta\sigma$ = 214 MPa, (0.29*fy)	0,1	214	107	131	306505	Centre, weld toe failure
3	AW	Aalto	S690QL	CA3, $\Delta\sigma$ = 180 MPa, (0.24*fy)	0,1	180	90	110	749647	Centre, weld toe failure
4	AW	Aalto	S690QL	CA5, $\Delta\sigma$ = 135 MPa, (0.18*fy)	0,1	135	68	83	1500000	Centre, weld toe failure
5	AW	Aalto	S690QL	CA2, $\Delta\sigma$ = 214 MPa, (0.29*fy)	0,1	214	107	131	400209	Centre, weld toe failure
6	AW	Aalto	S690QL	CA5, $\Delta\sigma$ = 135 MPa, (0.18*fy)	0,1	135	68	83	10000000	Interrupted
7	AW	Aalto	S690QL	CA1, $\Delta\sigma$ = 215 MPa, (0.18*fy)	-0,43	215	107	43	1135003	Centre, weld toe failure
8	AW	Aalto	S690QL	CA2, $\Delta\sigma$ = 180 MPa, (0.15*fy)	-0,43	180	90	36	1816014	Centre, weld toe failure
9	AW	Aalto	S690QL	CA3, $\Delta\sigma$ = 262 MPa, (0.22*fy)	-0,43	262	131	52	297852	Centre, weld toe failure
10	AW	Aalto	S690QL	CA1, $\Delta\sigma$ = 215 MPa, (0.18*fy)	-0,43	215	107	43	1201490	Centre, weld toe failure
11	AW	Aalto	S690QL	CA2, $\Delta\sigma$ = 180 MPa, (0.15*fy)	-0,43	180	90	36	1376684	Centre, weld toe failure
12	AW	Aalto	S690QL	CA3, $\Delta\sigma$ = 262 MPa, (0.22*fy)	-0,43	262	131	52	287255	Centre, weld toe failure
15	AW	EPFL	S690QL	VA1, σ_{max}= 338 Mpa, (0.40*fy)	-0,43	483	242	96	4862751	Centre, weld toe failure
16	AW	EPFL	S690QL	VA0, σ_{max}= 423 Mpa, (0.50*fy)	-0,43	605	302	121	1730193	Centre, weld toe failure
17	AW	EPFL	S690QL	VA1, σ_{max}= 338 Mpa, (0.40*fy)	-0,43	483	242	96	4449828	Centre, weld toe failure
18	AW	EPFL	S690QL	VA2, σ_{max}= 582 Mpa, (0.70*fy)	-0,43	832	416	166	602888	Centre, weld toe failure
19	AW	Aalto	S690QL	CA4, $\Delta\sigma$ = 188 MPa, (0.25*fy)	0,1	188	94	115	601000	Centre, weld toe failure
20	AW	Aalto	S690QL	CA5, $\Delta\sigma$ = 135 MPa, (0.18*fy)	0,1	135	68	83	10000000	Interrupted
24	AW	EPFL	S690QL	VA2, σ_{max}= 582 Mpa, (0.70*fy)	-0,43	832	416	166	464000	Centre, weld toe failure
2	HFMI	EPFL	S690QL	VA2, σ_{max}= 582 Mpa (0.7*fy)	-0,43	832	416	166	6579000	Centre, weld toe failure
3	HFMI	EPFL	S690QL	VA0, σ_{max}= 833 MPa, (1*fy)	-0,43	1190	595	237	492000	Centre, weld toe failure
4	HFMI	EPFL	S690QL	CA2, $\Delta\sigma$ = 310 MPa, (0.26*fy)	-0,43	310	155	62	17663658	Edge, gusset failure
5	HFMI	EPFL	S690QL	VA2, σ_{max}= 582 Mpa (0.7*fy)	-0,43	832	416	166	5466000	Edge, weld toe failure
6	HFMI	EPFL	S690QL	VA1, σ_{max}= 665 MPa, (0.8*fy)	-0,43	951	475	190	4788750	Centre, weld toe failure
7	HFMI	EPFL	S690QL	VA0, σ_{max}= 833 MPa, (1*fy)	-0,43	1190	595	237	346500	Centre, weld toe failure
8	HFMI	EPFL	S690QL	VA2, σ_{max}= 582 Mpa (0.7*fy)	-0,43	832	416	166	2499000	Edge, weld toe failure
9	HFMI	EPFL	S690QL	VA0, σ_{max}= 833 MPa, (1*fy)	-0,43	1190	595	237	258750	Centre, weld toe failure
12	HFMI	EPFL	S690QL	VA1, σ_{max}= 665 MPa, (0.8*fy)	-0,43	951	475	190	2565750	Edge, weld toe failure
13	HFMI	EPFL	S690QL	VA1, σ_{max}= 665 MPa, (0.8*fy)	-0,43	951	475	190	2637000	Edge, weld toe failure
14	HFMI	Aalto	S690QL	CA1, $\Delta\sigma$ = 357 MPa, (0.3*fy)	-0,43	357	179	71	3216516	Edge, weld toe failure
15	HFMI	EPFL	S690QL	CA0, $\Delta\sigma$ = 416 MPa, (0.35*fy)	-0,43	416	208	83	399875	Edge, weld toe failure
16	HFMI	EPFL	S690QL	CA2, $\Delta\sigma$ = 310 MPa, (0.26*fy)	-0,43	310	155	62	4881987	Interruptted
19	HFMI	Aalto	S690QL	CA3, $\Delta\sigma$ = 260 MPa, (0.22*fy)	-0,43	260	130	52	24325765	Interrupted
20	HFMI	EPFL	S690QL	CA2, $\Delta\sigma$ = 310 MPa, (0.26*fy)	-0,43	310	155	62	583126	Weld toe failure
21	HFMI	Aalto	S690QL	CA1, $\Delta\sigma$ = 357 MPa, (0.3*fy)	-0,43	357	179	71	707313	Edge, weld toe failure
22	HFMI	Aalto	S690QL	CA3, $\Delta\sigma$ = 260 MPa, (0.22*fy)	-0,43	260	130	52	29574017	Interrupted
23	HFMI	Aalto	S690QL	CA1, $\Delta\sigma$ = 357 MPa, (0.3*fy)	-0,43	357	179	71	622589	Edge, weld toe failure
24	HFMI	Aalto	S690QL	CA2, $\Delta\sigma$ = 310 MPa, (0.26*fy)	-0,43	310	155	62	1806193	Edge, weld toe failure

C. Appendix k_m factors for the non-load carrying transverse specimens

The stress magnification factor was calculated by Equation 1 for each specimen group. The maximum, minimum, average and standard deviation was derived and presented in Tables 17-16. The average values are also plotted in Figures 18 and 19 with k_m as y-axis and specimen as x-axis, respectively. Please note that Y-axis scale is not constant.

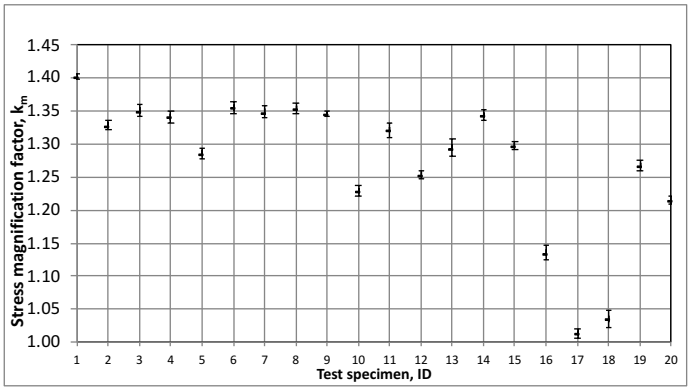

(a) As-welded condition

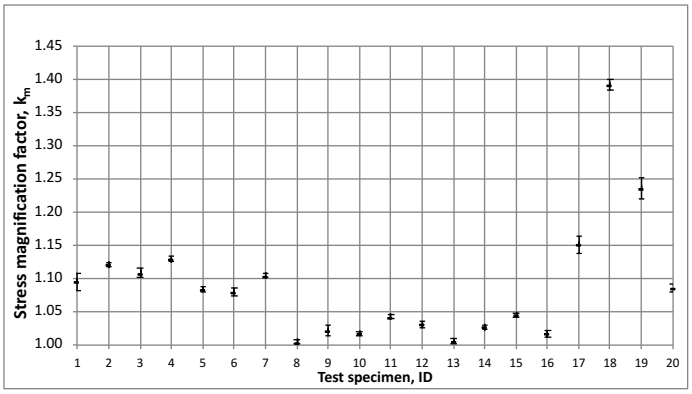

(b) HFMI-treated condition

Figure 18: Stress magnification factors k_m of non-load carrying transverse attachment for the AH36 steel grade

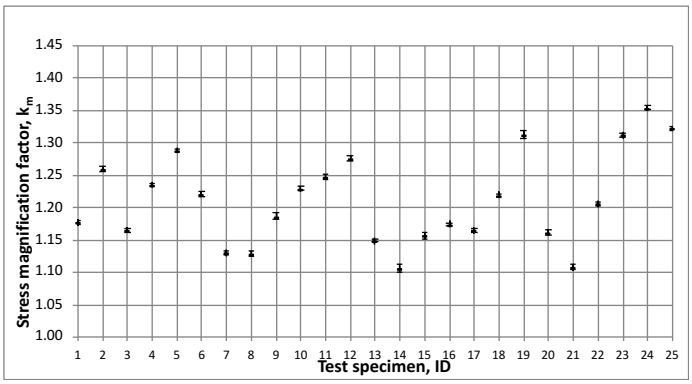

(a) As-welded condition

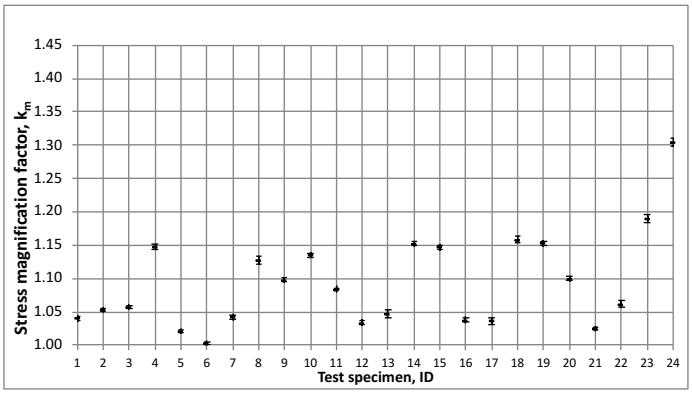

(b) HFMI-treated condition

Figure 19: Stress magnification factors k_m of non-load carrying transverse attachment for the S690QL steel grade

Table 15: Maximum, minimum, average and standard deviation of stress magnification factors for the as-welded condition of the AH36 steel grade

Specimen	$k_{m,max}$	$k_{m,min}$	$k_{m,avg}$	$k_{m,SD}$
1	1.41	1.40	1.40	0.0044
2	1.34	1.32	1.33	0.0066
3	1.37	1.34	1.35	0.0090
4	1.36	1.33	1.34	0.0091
5	1.31	1.28	1.29	0.0080
6	1.37	1.34	1.36	0.0085
7	1.37	1.34	1.35	0.0084
8	1.37	1.34	1.35	0.0083
9	1.35	1.34	1.35	0.0038
10	1.24	1.22	1.23	0.0081
11	1.35	1.30	1.32	0.0114
12	1.27	1.25	1.25	0.0059
13	1.31	1.28	1.29	0.0125
14	1.36	1.33	1.34	0.0078
15	1.31	1.29	1.30	0.0060
16	1.16	1.12	1.14	0.0107
17	1.03	1.00	1.01	0.0072
18	1.06	1.02	1.04	0.0124
19	1.28	1.25	1.27	0.0089
20	1.23	1.21	1.22	0.0066

Table 16: Maximum, minimum, average and standard deviation of stress magnification factors for the HFMI-treated condition of the AH36 steel grade

Specimen	$k_{m,max}$	$k_{m,min}$	$k_{m,avg}$	$k_{m,SD}$
1	1.11	1.07	1.10	0.0131
2	1.13	1.12	1.12	0.0031
3	1.12	1.10	1.11	0.0063
4	1.14	1.12	1.13	0.0038
5	1.09	1.08	1.08	0.0040
6	1.09	1.07	1.08	0.0058
7	1.11	1.10	1.10	0.0028
8	1.01	1.00	1.00	0.0037
9	1.04	1.01	1.02	0.0073
10	1.02	1.01	1.02	0.0028
11	1.05	1.04	1.04	0.0025
12	1.04	1.02	1.03	0.0041
13	1.01	1.00	1.01	0.0042
14	1.03	1.02	1.03	0.0035
15	1.05	1.04	1.05	0.0030
16	1.02	1.01	1.02	0.0046
17	1.18	1.13	1.15	0.0131
18	1.40	1.38	1.39	0.0085
19	1.26	1.21	1.24	0.0161
20	1.09	1.07	1.09	0.0058

Table 17: Maximum, minimum, average and standard deviation of stress magnification factor for the as-welded condition of the S690QL steel grade

Specimen	$k_{m,max}$	$k_{m,min}$	$k_{m,avg}$	$k_{m,SD}$
1	1.18	1.17	1.18	0.0027
2	1.26	1.25	1.26	0.0037
3	1.17	1.16	1.17	0.0028
4	1.24	1.23	1.24	0.0021
5	1.29	1.28	1.29	0.0026
6	1.23	1.22	1.22	0.0036
7	1.13	1.13	1.13	0.0028
8	1.14	1.12	1.13	0.0041
9	1.19	1.18	1.19	0.0047
10	1.23	1.22	1.23	0.0034
11	1.25	1.24	1.25	0.0040
12	1.28	1.27	1.28	0.0040
13	1.15	1.14	1.15	0.0019
14	1.12	1.10	1.11	0.0054
15	1.16	1.15	1.16	0.0053
16	1.18	1.17	1.17	0.0021
17	1.17	1.16	1.16	0.0024
18	1.22	1.21	1.22	0.0024
19	1.32	1.30	1.31	0.0058
20	1.17	1.16	1.16	0.0044
21	1.12	1.10	1.11	0.0041
22	1.21	1.20	1.21	0.0037
23	1.32	1.31	1.31	0.0037
24	1.36	1.35	1.35	0.0030
25	1.33	1.32	1.32	0.0031

Table 18: Maximum, minimum, average and standard deviation of stress magnification factor for the HFMI-treated condition of the S690QL steel grade

Specimen	$k_{m,max}$	$k_{m,min}$	$k_{m,avg}$	$k_{m,SD}$
1	1.05	1.04	1.04	0.0024
2	1.06	1.05	1.05	0.0029
3	1.06	1.05	1.06	0.0015
4	1.16	1.14	1.15	0.0039
5	1.03	1.02	1.02	0.0026
6	1.01	1.00	1.00	0.0028
7	1.05	1.03	1.04	0.0039
8	1.13	1.11	1.13	0.0066
9	1.10	1.09	1.10	0.0031
10	1.14	1.13	1.14	0.0032
11	1.09	1.08	1.08	0.0015
12	1.04	1.03	1.03	0.0030
13	1.06	1.04	1.05	0.0055
14	1.16	1.14	1.15	0.0031
15	1.16	1.14	1.15	0.0034
16	1.04	1.03	1.04	0.0028
17	1.04	1.03	1.04	0.0043
18	1.17	1.15	1.16	0.0052
19	1.16	1.15	1.15	0.0027
20	1.10	1.09	1.10	0.0029
21	1.03	1.02	1.03	0.0019
22	1.07	1.05	1.06	0.0048
23	1.20	1.18	1.19	0.0061
24	1.31	1.29	1.31	0.0061